

PSEUDOSCALAR MSSM HIGGS PRODUCTION AT NLO SUSY-QCD

Emanuele Bagnaschi¹, Lukas Fritz^{2,3}, Stefan Liebler^{4‡}, Margarete Mühlleitner⁴, Thanh Tien Dat Nguyen⁴ and Michael Spira²

¹ *Theoretical Physics Department, CERN, CH-1211 Geneva 23, Switzerland*

² *Paul Scherrer Institut, CH-5232 Villigen PSI, Switzerland*

³ *Institut für Theoretische Physik, Zurich University, CH-8057 Zurich, Switzerland*

⁴ *Institute for Theoretical Physics, Karlsruhe Institute of Technology, D-76128 Karlsruhe, Germany*

Abstract

One of the most important mechanisms at the Large Hadron Collider (LHC) for the production of the pseudoscalar Higgs boson of the Minimal Supersymmetric Standard Model (MSSM) is the loop-induced gluon fusion process $gg \rightarrow A$. The higher-order QCD corrections have been obtained a long time ago and turned out to be large. However, the genuine supersymmetric (SUSY-)QCD corrections have been obtained only in the limit of large SUSY particle masses so far. We describe our calculation of the next-to-leading-order (NLO) SUSY-QCD results with full mass dependence and present numerical results for a few representative benchmark points. We also address the treatment of the effective top and bottom Yukawa couplings, in the case of heavy SUSY particles, in terms of effective low-energy theories where the heavy degrees of freedom have been decoupled. Furthermore, we include a discussion of the relation between the SUSY-QCD corrections that we have computed and the Adler-Bardeen theorem for the axial anomaly. In addition, we apply our results to the gluonic and photonic pseudoscalar Higgs decays $A \rightarrow gg, \gamma\gamma$ at NLO.

1 Introduction

The discovery of a Standard-Model-like Higgs boson at the LHC [1] completed the Standard Model (SM) of electroweak and strong interactions. The existence of the Higgs boson [2] is inherently related to the mechanism of spontaneous symmetry breaking while preserving the full gauge symmetry and the renormalizability of the SM [3]. The measured Higgs boson mass of (125.09 ± 0.24) GeV [4] ranks at the weak scale. The existence of the Higgs boson allows the SM particles to be weakly interacting up to high-energy scales [5]. This, however, is only possible for particular Higgs-boson couplings to all other particles, so that the knowledge of the Higgs-boson mass fixes all its properties uniquely. The massive gauge bosons and fermions acquire mass through their interaction with the Higgs field that develops a vacuum

[‡] Former academic affiliation

expectation value in its ground state. The minimal model requires the introduction of one isospin Higgs doublet and leads after spontaneous symmetry breaking to the existence of one scalar Higgs boson. The SM itself, however, leaves several fundamental questions open as e.g. the nature of Dark Matter, the baryon asymmetry of the universe or the stability of the electroweak against the Planck or grand unification scale. If the SM is extended to a Grand Unified Theory (GUT) scale, radiative corrections to the Higgs-boson mass tend to push it towards the GUT scale, if the Higgs boson couples to particles of that mass order. In order to obtain a Higgs mass at the electroweak scale the Higgs-mass counterterm has to be fine-tuned to cancel these large corrections thus establishing an unnatural situation that asks for a solution. This is known as the hierarchy problem [6]. These open questions call for extensions of the minimal model. To increase the experimental sensitivity to effects beyond the SM (BSM), the SM and BSM parts of measured relevant observables need to be known as precisely as possible in order to allow for a reliable interpretation of potential deviations and effects beyond the SM.

The open problems of the SM motivate extensions of the minimal model which cover e.g. the Two-Higgs-Doublet model (2HDM) [7] or the minimal supersymmetric extension (MSSM) [8, 9] as prominent and highly motivated examples. Supersymmetric extensions of the SM provide a solution to the hierarchy problem if the supersymmetric particle masses rank at scales up to a few TeV [10]. Supersymmetry relates fermionic and bosonic degrees of freedom and thus links internal and external symmetries. The MSSM, if embedded in a Grand Unified Theory, predicts a value of the Weinberg angle in excellent agreement with experimental measurements of electroweak precision observables [11]. Moreover, it contains a Dark Matter candidate if R-parity is conserved [12] and allows for generating electroweak symmetry breaking radiatively, since the top mass ranks in the proper region for that mechanism to work [13]. The MSSM introduces two isospin Higgs doublets due to the analyticity of the superpotential, requiring two different doublets for the generation of the up- and down-type fermion masses and the anomaly-freedom with respect to the gauge symmetries [14], since the higgsino states as the supersymmetric partners of the Higgs bosons contribute to the Adler-Bell-Jackiw anomaly [15]. Due to this, the MSSM Higgs sector is a 2HDM of type II at leading order (LO). There are a light (h) and heavy (H) scalar, a pseudoscalar (A) and two charged (H^\pm) states as the corresponding mass eigenstates. Since the self-interactions of the Higgs fields, as defined by the corresponding Higgs potential, are entirely fixed by the electroweak gauge couplings, this induces an upper bound on the light scalar Higgs mass that has to be smaller than the Z -boson mass M_Z at LO. However, radiative corrections, which are dominated by top-quark-induced contributions, strongly increase this upper bound to about 130 GeV in general [16]. The Higgs sector is uniquely fixed at LO by the value of the pseudoscalar mass M_A and the parameter $\tan\beta$, defined as the ratio of the two vacuum expectation values of the scalar Higgs fields.

In this work, we will describe the calculation of the full SUSY-QCD corrections at NLO to pseudoscalar Higgs production via the gluon-fusion mechanism $gg \rightarrow A$. This process belongs to the dominant MSSM Higgs-boson production processes at the LHC and thus contributes to the present bounds on the so far negative searches for the heavy MSSM Higgs bosons at the LHC. In order to make the predictions for this process reliable, the full NLO

corrections within SUSY–QCD have to be computed. The paper is organized as follows. In Section 2, we will summarize the present status of the gluon-fusion cross section. In Section 3, we briefly discuss pseudoscalar Higgs decays to gluons and photons. In Section 4 we will describe our implementation of the stop and sbottom sector followed by the detailed description of our NLO calculation in Section 5. In the latter we also include a discussion of effective Yukawa couplings and the relation of the considered process to the Adler–Bardeen theorem [17]. In Section 6, we discuss numerical results for a few representative benchmark points. We close the paper with our conclusions in Section 7.

2 Gluon Fusion

The dominant channels for pseudoscalar production at a hadron collider are given by gluon fusion, $gg \rightarrow A$, and production in association with bottom quarks, $q\bar{q}, gg \rightarrow Abb$, with their relative importance depending on the value of $\text{tg}\beta$. For large $\text{tg}\beta$, Abb production dominates, with the gluon fusion contribution amounting to up to about 30% close to the present exclusion bounds, depending on the region in the $M_A - \text{tg}\beta$ plane [18, 19].

2.1 Leading Order

The gluon-fusion mechanism [20]

$$pp \rightarrow gg \rightarrow A$$

dominates the pseudoscalar MSSM Higgs boson production at the LHC in the phenomenologically relevant Higgs mass ranges for small and moderate values of $\text{tg}\beta$. Only for large $\text{tg}\beta$ the associated Abb production channel develops a larger cross section due to the enhanced Higgs couplings to bottom quarks [21]. The gluon coupling to pseudoscalar Higgs bosons in the MSSM is built up by loops involving top and bottom quarks, see Fig. 1. The partonic

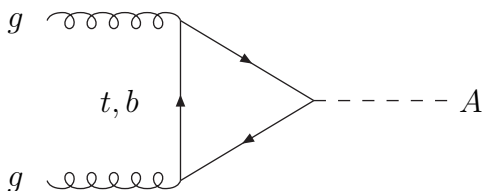


Figure 1: *Typical diagram contributing to $gg \rightarrow A$ at lowest order.*

cross section is given at lowest order by [22, 23]:

$$\begin{aligned} \hat{\sigma}_{LO}^A(gg \rightarrow A) &= \sigma_0^A \delta(1-z) \\ \sigma_0^A &= \frac{G_F \alpha_s^2(\mu_R)}{128\sqrt{2}\pi} \left| \sum_Q g_Q^A A_Q^A(\tau_Q) \right|^2, \end{aligned} \quad (1)$$

where G_F denotes the Fermi constant, α_s the strong coupling, and μ_R the renormalization scale. The scaling variables are defined as $z = M_A^2/\hat{s}$, $\tau_Q = 4M_Q^2/M_A^2$ ($Q = t, b$), and \hat{s} denotes the partonic c.m. energy squared. The amplitudes $A_Q^A(\tau_Q)$ are obtained as

$$A_Q^A(\tau) = \tau f(\tau)$$

$$f(\tau) = \begin{cases} \arcsin^2 \frac{1}{\sqrt{\tau}} & \tau \geq 1 \\ -\frac{1}{4} \left[\log \frac{1 + \sqrt{1-\tau}}{1 - \sqrt{1-\tau}} - i\pi \right]^2 & \tau < 1 \end{cases} \quad (2)$$

and the MSSM coupling factors g_Q^A are determined as $g_t^A = 1/\text{tg}\beta$, $g_b^A = \text{tg}\beta$. In the narrow-width approximation the hadronic cross section is given by

$$\sigma_{LO}(pp \rightarrow A) = \sigma_0^A \tau_A \frac{d\mathcal{L}^{gg}}{d\tau_A} \quad (3)$$

with the scaling variable $\tau_A = M_A^2/s$, where s specifies the total hadronic c.m. energy squared, and the gluon luminosity

$$\frac{d\mathcal{L}^{gg}}{d\tau} = \int_{\tau}^1 \frac{dx}{x} g(x, \mu_F^2) g(\tau/x, \mu_F^2) \quad (4)$$

at the factorization scale μ_F . For small $\text{tg}\beta$ the top-loop contribution is dominant, while for large values of $\text{tg}\beta$ the bottom-quark contribution is strongly enhanced.

2.2 QCD Corrections

The full two-loop QCD corrections to the gluon-fusion cross section were calculated in the past [23, 24, 25]. In complete analogy to the SM case, they consist of virtual two-loop corrections to the basic $gg \rightarrow A$ process and real one-loop corrections due to the associated production of the pseudoscalar Higgs boson with massless quarks and gluons. The final result for the hadronic cross section at NLO can be decomposed as

$$\sigma(pp \rightarrow A + X) = \sigma_0^A \left[1 + C^A \frac{\alpha_s}{\pi} \right] \tau_A \frac{d\mathcal{L}^{gg}}{d\tau_A} + \Delta\sigma_{gg}^A + \Delta\sigma_{gq}^A + \Delta\sigma_{q\bar{q}}^A. \quad (5)$$

The analytical expressions for arbitrary Higgs boson and quark masses at NLO are rather involved [23, 25]. As in the SM case, the quark-loop masses have been identified with the pole mass m_Q ($Q = t, b$), while the QCD coupling and the parton distribution functions (PDFs) of the proton are treated in the $\overline{\text{MS}}$ scheme with five active flavours. The axial γ_5 coupling can be regularized in the 't Hooft–Veltman scheme [26] or its extension by Larin [27], which preserve the chiral symmetry in the massless quark limit by the addition of supplementary counterterms and fulfill the non-renormalization theorem [17] of the ABJ anomaly [15] at vanishing momentum transfer. The same result can also be obtained with the scheme of Ref. [28] that gives up the cyclicity of the traces involving Clifford matrices. The next-to-next-to-leading order (NNLO) QCD corrections have been obtained in the limit of heavy

top quarks (HTL) [29]. The QCD corrections are positive and large in total, increasing the MSSM Higgs production cross sections at the LHC by up to about 100%. For the top-loop contributions alone, the (moderate) NNLO corrections in the heavy-top limit (HTL) can be used consistently. Electroweak corrections are unknown so far.

The leading terms of the relative QCD corrections in the HTL provide a reasonable approximation for small $\text{tg}\beta$ up to pseudoscalar Higgs masses of ~ 1 TeV with a maximal deviation of $\sim 25\%$ for $\text{tg}\beta \lesssim 5$ at NLO in the intermediate mass range [30]. The genuine SUSY–QCD corrections are only known in the limit of heavy SUSY particles [31, 32]. For large values of $\text{tg}\beta$ they can be large and approximated by the Δ_b terms. This work improves this incomplete status by calculating the full SUSY–QCD corrections with full virtual quark-, squark- and gluino-mass dependence, which will contribute to the virtual corrections as

$$C^A = C_{QCD}^A + C_{SQCD}^A \quad (6)$$

where C_{QCD}^A is the virtual part of the pure QCD corrections. We will compare the full results for C_{SQCD}^A with the approximate calculations in the following sections. For the SUSY–QCD corrections we implement the stop and sbottom sector at the NLO level, although the squarks do not contribute at LO, and therefore the definition of a renormalization scheme for their parameters is not required. However, to be in line with the treatment of scalar Higgs production in a future work, where stops and sbottoms contribute at LO already, we choose the same framework. The NLO implementation of the stop and sbottom sectors will be discussed in Section 4.

In the opposite limit, where the pseudoscalar Higgs mass is much larger than the quark mass, the analytical results of the relative QCD corrections coincide with the SM expressions at the leading and subleading logarithmic level for both the scalar and pseudoscalar Higgs bosons up to NLO where the results for small quark masses are known [23]. This coincidence is due to the restoration of the chiral symmetry in the massless quark limit. The leading double and subleading logarithms have been resummed recently [33].

3 Pseudoscalar Higgs Decays

Although pseudoscalar Higgs decays into gluons and photons do not play a prominent role as for the SM-like light scalar Higgs particle, they can still reach sizeable branching ratios for smaller values of $\text{tg}\beta$ so that they might be accessible at future e^+e^- colliders.

3.1 $A \rightarrow gg$

The decay of pseudoscalar Higgs bosons into gluons is loop-induced, see Fig. 2. The dominant contributions originate from top and bottom loops, while lighter quarks as e.g. the charm quark yield contributions at the per-cent or sub-per-cent level only. The LO expression of the gluonic pseudoscalar Higgs decay reads [22, 23]

$$\Gamma_{LO}(A \rightarrow gg) = \frac{G_F \alpha_s^2 M_A^3}{16\sqrt{2}\pi^3} \left| \sum_Q g_Q^A A_Q^A(\tau_Q) \right|^2, \quad (7)$$

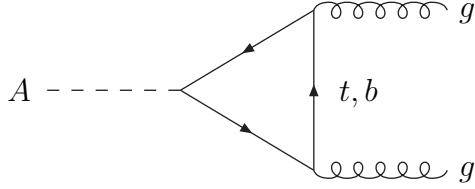


Figure 2: Typical diagrams contributing to $A \rightarrow gg$ at lowest order.

where we adopted the same notation as in Eq. (1) using the same quark form factors as given in Eq. (2). The NLO QCD and SUSY-QCD corrections can be cast into the form

$$\Gamma(A \rightarrow gg) = \Gamma_{LO} \left\{ 1 + E^A \frac{\alpha_s}{\pi} \right\}, \quad (8)$$

with the NLO coefficient E^A splitting into pure QCD corrections and genuine SUSY-QCD corrections,

$$E^A = E_{QCD}^A + E_{SQCD}^A. \quad (9)$$

The QCD part can be expressed as [23, 34]

$$E_{QCD}^A = \frac{97}{4} - \frac{7}{6} N_F + \Delta_m, \quad (10)$$

where Δ_m denotes finite mass effects at NLO [23], and N_F is the number of active light flavors included as final-state quarks as well. For e.g. $\text{tg}\beta = 1$ the mass effects amount to $\Delta_m \approx 1.3$, if the quark masses are defined as pole masses, but are larger for increasing values of $\text{tg}\beta$ due to the rising significance of the bottom contributions. The expression without Δ_m corresponds to the heavy-quark limit of the relative QCD corrections. The coefficient E_{SQCD}^A coincides with the one for the gluon-fusion cross section of Eq. (6),

$$E_{SQCD}^A = C_{SQCD}^A. \quad (11)$$

3.2 $A \rightarrow \gamma\gamma$

As for the gluonic pseudoscalar Higgs decay, its decay into photon pairs is a loop-induced process with top and bottom quarks providing the dominant contributions, but also charginos, see Fig. 3. At LO, the pseudoscalar decay width into photon pairs reads [22, 23]

$$\Gamma_{LO}(A \rightarrow \gamma\gamma) = \frac{G_F \alpha^2 M_A^3}{32\sqrt{2}\pi^3} \left| \sum_f N_{cf} e_f^2 g_f^A A_f^A(\tau_f) + \sum_{\tilde{\chi}^\pm} g_{\tilde{\chi}^\pm}^A A_{\tilde{\chi}^\pm}^A(\tau_{\tilde{\chi}^\pm}) \right|^2, \quad (12)$$

where $\tilde{\chi}^\pm$ denotes the two chargino mass eigenstates, N_{cf} is the color factor of the fermions of charge e_f contributing to the loops. The LO form factors $A_i^A(\tau_i)$ ($i = t, b, \tilde{\chi}^\pm$) follow the

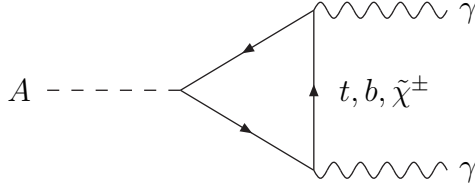


Figure 3: *Generic diagrams contributing to $A \rightarrow \gamma\gamma$ at LO.*

expressions of Eq. (2). The chargino-coupling factors are given by

$$g_{\tilde{\chi}_i^\pm} = -2 \frac{M_W}{m_{\tilde{\chi}_i^\pm}} (S_{ii} \cos \beta + Q_{ii} \sin \beta), \quad (13)$$

with the charge factors $Q_{ii}, S_{ii} (i = 1, 2)$ given in Refs. [9, 22]. They are related to the mixing angles between the chargino states $\tilde{\chi}_{1,2}^\pm$. The NLO QCD and SUSY-QCD corrections can be defined as a shift of the corresponding LO quark-form factors,

$$A_Q^A(\tau_Q) \rightarrow A_Q^A(\tau_Q) \left\{ 1 + [\mathcal{D}_{Q,QCD}^A + \mathcal{D}_{Q,SQCD}^A] \frac{\alpha_s}{\pi} \right\} \quad (14)$$

where the pure QCD corrections $\mathcal{D}_{Q,QCD}$ to the quark form factor vanish in the heavy-quark limit due to the Adler-Bardeen [17] theorem for these leading contributions. This means they are induced by pure quark-mass effects [23]. The implementation of the QCD corrections $\mathcal{D}_{Q,QCD}^A$ follows Ref. [23], i.e. the running quark masses

$$\begin{aligned} \hat{m}_Q(\mu) &= \kappa(m_Q) \overline{m}_Q(\mu) \\ \kappa(m_Q) &= 1 + \frac{4}{3} \frac{\alpha_s(m_Q)}{\pi} + K_Q \left(\frac{\alpha_s(m_Q)}{\pi} \right)^2 + \mathcal{O}(\alpha_s^3) \\ \overline{m}_Q(\mu) &= \overline{m}_Q(m_Q) \frac{c[\alpha_s(\mu)/\pi]}{c[\alpha_s(m_Q)/\pi]} \\ c(x) &= \left(\frac{7}{2} x \right)^{\frac{4}{7}} [1 + 1.398x + 1.793x^2 - 0.6834x^3] \quad \text{for } m_t < \mu \\ &= \left(\frac{23}{6} x \right)^{\frac{12}{23}} [1 + 1.175x + 1.501x^2 + 0.1725x^3] \quad \text{for } m_b < \mu < m_t \end{aligned} \quad (15)$$

where $\overline{m}_Q(\mu)$ denotes the $\overline{\text{MS}}$ mass [35] and $K_b = 12.4, K_t = 10.9$ [36], are used for the loop-quark masses at the scale $\mu = M_A/2$ such that the relations $M_A = 2\hat{m}_Q(m_Q) = 2m_Q$ ($Q = t, b$) define the virtual quark thresholds in terms of the quark pole masses m_Q . The genuine SUSY-QCD corrections, represented by the coefficient $\mathcal{D}_{Q,SQCD}^A$, will be discussed in Section 6.3.

4 Squark Masses and Couplings

In the following the parametrization of the stop and sbottom sectors will be described in detail at LO and at NLO starting from the soft SUSY-breaking parameters, where the extension to NLO requires a dedicated scheme choice for our gluon-fusion calculation. We will follow the set-ups described in Refs. [37, 38] with corresponding modifications.

4.1 Sfermion Masses and Couplings at LO

Since the scalar sfermion current-eigenstates $\tilde{f}_{L,R}$, the super-partners of the left- and right-handed fermions, mix with each other, the corresponding mass eigenstates $\tilde{f}_{1,2}$ are related to the current eigenstates by a rotation involving the mixing angles θ_f ,

$$\begin{aligned}\tilde{f}_1 &= \tilde{f}_L \cos \theta_f + \tilde{f}_R \sin \theta_f \\ \tilde{f}_2 &= -\tilde{f}_L \sin \theta_f + \tilde{f}_R \cos \theta_f,\end{aligned}\tag{16}$$

These mixing angles grow with the Yukawa couplings of the corresponding SM fermions, i.e. mixing effects are in general only relevant for the third-generation sfermions $\tilde{t}, \tilde{b}, \tilde{\tau}$. The mass matrix in the current-eigenstate basis is given by

$$\mathcal{M}_{\tilde{f}} = \begin{bmatrix} \tilde{M}_{\tilde{f}_L}^2 + m_f^2 & m_f(A_f - \mu r_f) \\ m_f(A_f - \mu r_f) & \tilde{M}_{\tilde{f}_R}^2 + m_f^2 \end{bmatrix}.\tag{17}$$

where $r_b = r_\tau = 1/r_t = \text{tg}\beta$. A_f is the trilinear sfermion coupling of the soft SUSY-breaking part of the Lagrangian, while μ denotes the higgsino mass parameter and m_f the fermion mass. The parameters $\tilde{M}_{\tilde{f}_{L/R}}$ absorb the corresponding D -terms,

$$\begin{aligned}\tilde{M}_{\tilde{f}_{L/R}}^2 &= M_{\tilde{f}_{L/R}}^2 + D_{\tilde{f}_{L/R}} \\ D_{\tilde{f}_L} &= M_Z^2(I_{3L}^f - e_f \sin^2 \theta_W) \cos 2\beta \\ D_{\tilde{f}_R} &= M_Z^2 e_f \sin^2 \theta_W \cos 2\beta,\end{aligned}\tag{18}$$

with e_f being the electric charge of the sfermion, and I_{3L} its third isospin component, θ_W denotes the Weinberg angle and $M_{\tilde{f}_{L/R}}$ are the sfermion mass parameters of the soft SUSY-breaking part of the Lagrangian. Hence, the mixing angles are determined from

$$\sin 2\theta_f = \frac{2m_f(A_f - \mu r_f)}{m_{\tilde{f}_1}^2 - m_{\tilde{f}_2}^2}, \quad \cos 2\theta_f = \frac{\tilde{M}_{\tilde{f}_L}^2 - \tilde{M}_{\tilde{f}_R}^2}{m_{\tilde{f}_1}^2 - m_{\tilde{f}_2}^2}\tag{19}$$

and the squark-eigenstate masses acquire the form

$$m_{\tilde{f}_{1,2}}^2 = m_f^2 + \frac{1}{2} \left[\tilde{M}_{\tilde{f}_L}^2 + \tilde{M}_{\tilde{f}_R}^2 \mp \sqrt{(\tilde{M}_{\tilde{f}_L}^2 - \tilde{M}_{\tilde{f}_R}^2)^2 + 4m_f^2(A_f - \mu r_f)^2} \right].\tag{20}$$

In the current-eigenstate basis, the neutral Higgs couplings to sfermions are given by

$$\begin{aligned}
g_{\tilde{f}_L \tilde{f}_L}^\Phi &= m_f^2 g_1^\Phi + M_Z^2 (I_{3f} - e_f \sin^2 \theta_W) g_2^\Phi \\
g_{\tilde{f}_R \tilde{f}_R}^\Phi &= m_f^2 g_1^\Phi + M_Z^2 e_f \sin^2 \theta_W g_2^\Phi \\
g_{\tilde{f}_L \tilde{f}_R}^\Phi &= \frac{m_f}{2} (\mu g_3^\Phi - A_f g_4^\Phi),
\end{aligned} \tag{21}$$

where the couplings g_i^Φ ($i = 1, \dots, 4$) are specified in Table 1. In case of the scalar Higgs bosons h, H the couplings to sfermions are symmetric, i.e. $g_{\tilde{f}_R \tilde{f}_L}^{h,H} = g_{\tilde{f}_L \tilde{f}_R}^{h,H}$, while for the pseudoscalar Higgs boson A the diagonal couplings $g_{\tilde{f}_L \tilde{f}_L}^A$ and $g_{\tilde{f}_R \tilde{f}_R}^A$ vanish and the off-diagonal couplings are antisymmetric, $g_{\tilde{f}_R \tilde{f}_L}^A = -g_{\tilde{f}_L \tilde{f}_R}^A$. The physical Higgs couplings to the sfermion mass eigenstates $\tilde{f}_{1,2}$ read

$$\begin{aligned}
g_{\tilde{f}_1 \tilde{f}_1}^{h,H} &= g_{\tilde{f}_L \tilde{f}_L}^{h,H} \cos^2 \theta_f + g_{\tilde{f}_R \tilde{f}_R}^{h,H} \sin^2 \theta_f + g_{\tilde{f}_L \tilde{f}_R}^{h,H} \sin 2\theta_f \\
g_{\tilde{f}_2 \tilde{f}_2}^{h,H} &= g_{\tilde{f}_L \tilde{f}_L}^{h,H} \sin^2 \theta_f + g_{\tilde{f}_R \tilde{f}_R}^{h,H} \cos^2 \theta_f - g_{\tilde{f}_L \tilde{f}_R}^{h,H} \sin 2\theta_f \\
g_{\tilde{f}_1 \tilde{f}_2}^{h,H} &= g_{\tilde{f}_2 \tilde{f}_1}^{h,H} = \frac{1}{2} (g_{\tilde{f}_R \tilde{f}_R}^{h,H} - g_{\tilde{f}_L \tilde{f}_L}^{h,H}) \sin 2\theta_f + g_{\tilde{f}_L \tilde{f}_R}^{h,H} \cos 2\theta_f \\
g_{\tilde{f}_1 \tilde{f}_1}^A &= g_{\tilde{f}_2 \tilde{f}_2}^A = 0 \\
g_{\tilde{f}_1 \tilde{f}_2}^A &= -g_{\tilde{f}_2 \tilde{f}_1}^A = g_{\tilde{f}_L \tilde{f}_R}^A.
\end{aligned} \tag{22}$$

Next, we will discuss the extension of the stop and sbottom sectors to the NLO SUSY-QCD level.

\tilde{f}	Φ	g_1^Φ	g_2^Φ	g_3^Φ	g_4^Φ
\tilde{u}	h	$\cos \alpha / \sin \beta$	$-\sin(\alpha + \beta)$	$-\sin \alpha / \sin \beta$	$\cos \alpha / \sin \beta$
	H	$\sin \alpha / \sin \beta$	$\cos(\alpha + \beta)$	$\cos \alpha / \sin \beta$	$\sin \alpha / \sin \beta$
	A	0	0	1	$-1/\text{tg} \beta$
\tilde{d}	h	$-\sin \alpha / \cos \beta$	$-\sin(\alpha + \beta)$	$\cos \alpha / \cos \beta$	$-\sin \alpha / \cos \beta$
	H	$\cos \alpha / \cos \beta$	$\cos(\alpha + \beta)$	$\sin \alpha / \cos \beta$	$\cos \alpha / \cos \beta$
	A	0	0	1	$-\text{tg} \beta$

Table 1: *Coefficients of the neutral MSSM Higgs couplings to sfermion pairs. The symbols \tilde{u}, \tilde{d} denote up- and down-type sfermions.*

4.2 Stops and Sbottoms at NLO

At NLO, we will introduce the soft SUSY-breaking parameters in the $\overline{\text{MS}}$ scheme, i.e. we will start from the soft supersymmetry-breaking parameters $\overline{M}_{\tilde{Q}_{L,R}}(Q_0)$ and $\overline{A}_Q(Q_0)$ at the

input scale Q_0 which will in general be the SUSY scale, i.e. the average size of the left- and right-handed soft SUSY-breaking mass parameters. The benchmark scenarios of Ref. [19], however, are defined in the on-shell scheme of all involved input parameters. Thus, we will describe how we are implementing the relation between the $\overline{\text{MS}}$ and the on-shell parameters.

The bottom and top masses involved in the sbottom and stop mass matrices have to be chosen such that large higher-order corrections to their entries are avoided. We have chosen the top pole mass and a derived bottom mass for the sbottom mass matrix according to Refs. [38]. At LO, the stop/sbottom mass matrix is then given by ($q = t, b$)

$$\mathcal{M}_{\tilde{Q}} = \begin{bmatrix} \tilde{M}_{\tilde{Q}_L}^2(Q_0) + m_q^2 & m_q[\bar{A}_Q(Q_0) - \mu r_Q] \\ m_q[\bar{A}_Q(Q_0) - \mu r_Q] & \tilde{M}_{\tilde{Q}_R}^2(Q_0) + m_q^2 \end{bmatrix}, \quad (23)$$

where m_t is the top pole mass and m_b is the derived bottom mass as will be discussed in the following. The D -terms $D_{\tilde{Q}_{L/R}}$ have again been absorbed in the soft SUSY-breaking parameters, $\tilde{M}_{\tilde{Q}_{L/R}}(Q_0)$,

$$\tilde{M}_{\tilde{Q}_{L/R}}^2(Q_0) = \overline{M}_{\tilde{Q}_{L/R}}^2(Q_0) + D_{\tilde{Q}_{L/R}}. \quad (24)$$

The diagonal and off-diagonal entries of the stop/sbottom mass matrix are corrected at higher orders. We absorb the radiative corrections to the diagonal matrix elements in shifted soft mass parameters, $M_{\tilde{Q}_{L/R}}$,

$$M_{\tilde{Q}_{L/R}}^2 = \overline{M}_{\tilde{Q}_{L/R}}^2(Q_0) + \Delta \overline{M}_{\tilde{Q}_{L/R}}^2, \quad \tilde{M}_{\tilde{Q}_{L/R}}^2 = \tilde{M}_{\tilde{Q}_{L/R}}^2(Q_0) + \Delta \overline{M}_{\tilde{Q}_{L/R}}^2, \quad (25)$$

while the corrections to the off-diagonal entries will be absorbed in shifted soft trilinear couplings,

$$A_Q = \overline{A}_Q(Q_0) + \Delta \overline{A}_Q. \quad (26)$$

The shifted parameters are related to the radiative corrections to the mixing angles and stop/sbottom masses in order to arrive at simple tree-level like expressions at NLO for the stop/sbottom parameters. On the other hand, these shifted parameters correspond to the on-shell scheme introduced in Refs. [38] and thus have to coincide with the input values of the chosen benchmark scenario.

4.2.1 Stops

Starting from the on-shell parameters the treatment of the stop sector is identical to the LO level discussed before. The relation of the on-shell to the $\overline{\text{MS}}$ parameters, however, is affected by the NLO corrections.

At tree-level, the mixing angle $\tilde{\theta}_Q$ is derived from

$$\sin 2\tilde{\theta}_Q = \frac{2m_q[\bar{A}_Q(Q_0) - \mu r_Q]}{m_{\tilde{Q}_1}^2 - m_{\tilde{Q}_2}^2}, \quad \cos 2\tilde{\theta}_Q = \frac{\tilde{M}_{\tilde{Q}_L}^2(Q_0) - \tilde{M}_{\tilde{Q}_R}^2(Q_0)}{m_{\tilde{Q}_1}^2 - m_{\tilde{Q}_2}^2}, \quad (27)$$

where the tree-level squark masses $m_{\tilde{q}_{1/2}}$ according to Eq. (20) have been used¹.

¹The standard range for the squark mixing angle is chosen between 0 and π .

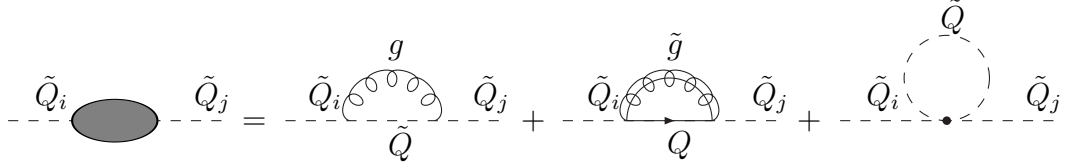


Figure 4: One-loop contributions to the squark self-energies.

The masses of the stop/sbottom mass eigenstates acquire radiative corrections,

$$\begin{aligned}
m_{\tilde{Q}_{1/2}}^2 &= m_Q^2 + \frac{1}{2} \left[\tilde{M}_{\tilde{Q}_L}^2(Q_0) + \tilde{M}_{\tilde{Q}_R}^2(Q_0) \right. \\
&\quad \left. \mp \sqrt{[\tilde{M}_{\tilde{Q}_L}^2(Q_0) - \tilde{M}_{\tilde{Q}_R}^2(Q_0)]^2 + 4m_Q^2[\bar{A}_Q(Q_0) - \mu r_Q]^2} \right] + \Delta m_{\tilde{Q}_{1/2}}^2 \\
\Delta m_{\tilde{Q}_{1/2}}^2 &= \Sigma_{11/22}(m_{\tilde{Q}_{1/2}}^2) + \delta \hat{m}_{\tilde{Q}_{1/2}}^2. \tag{28}
\end{aligned}$$

The self-energies $\Sigma_{11/22}$ of the stops/sbottoms can be derived from the diagrams in Fig. 4,

$$\begin{aligned}
\Sigma_{11/22}(m_{\tilde{Q}_{1/2}}^2) &= C_F \frac{\alpha_s}{\pi} \frac{1}{4} \left\{ -(1 + \cos^2 2\tilde{\theta}_Q) A_0(m_{\tilde{Q}_{1/2}}) - \sin^2 2\tilde{\theta}_Q A_0(m_{\tilde{Q}_{2/1}}) \right. \\
&\quad \left. + 2A_0(M_{\tilde{g}}) + 2A_0(m_Q) + 4m_{\tilde{Q}_{1/2}}^2 B_0(m_{\tilde{Q}_{1/2}}^2; 0, m_{\tilde{Q}_{1/2}}) \right. \\
&\quad \left. + 2 \left[M_{\tilde{g}}^2 + m_Q^2 - m_{\tilde{Q}_{1/2}}^2 \mp 2M_{\tilde{g}}m_Q \sin 2\tilde{\theta}_Q \right] B_0(m_{\tilde{Q}_{1/2}}^2; M_{\tilde{g}}, m_Q) \right\}, \tag{29}
\end{aligned}$$

where $M_{\tilde{g}}$ denotes the gluino mass and the scalar one-loop integrals are defined as ($n = 4 - 2\epsilon$) [39]

$$\begin{aligned}
A_0(m) &= \int \frac{d^n k}{(2\pi)^n} \frac{-i(4\pi)^2 \bar{\mu}^{2\epsilon}}{k^2 - m^2} \\
B_0(p^2; m_1, m_2) &= \int \frac{d^n k}{(2\pi)^n} \frac{-i(4\pi)^2 \bar{\mu}^{2\epsilon}}{[k^2 - m_1^2][(k+p)^2 - m_2^2]} \\
B_1(p^2; m_1, m_2) &= \frac{1}{2p^2} \left\{ A_0(m_1) - A_0(m_2) - (p^2 + m_1^2 - m_2^2) B_0(p^2; m_1, m_2) \right\}. \tag{30}
\end{aligned}$$

The scale $\bar{\mu}$ denotes the 't Hooft mass of dimensional regularization. The mass counterterms $\delta \hat{m}_{\tilde{Q}_{1,2}}^2$ of Eq. (28) are related to the counterterms of the input parameters,

$$\begin{aligned}
\delta \hat{m}_{\tilde{Q}_{1/2}}^2 &= 2m_Q \delta m_Q + \frac{1}{2} \left\{ \delta \bar{M}_{\tilde{Q}_L}^2 + \delta \bar{M}_{\tilde{Q}_R}^2 \pm \left[(\delta \bar{M}_{\tilde{Q}_L}^2 - \delta \bar{M}_{\tilde{Q}_R}^2) \cos 2\tilde{\theta}_Q \right. \right. \\
&\quad \left. \left. + \left(\frac{\delta m_Q}{m_Q} + \frac{\delta \bar{A}_Q}{\bar{A}_Q(Q_0) - \mu r_Q} \right) (m_{\tilde{Q}_1}^2 - m_{\tilde{Q}_2}^2) \sin^2 2\tilde{\theta}_Q \right] \right\} \\
&= -C_F \frac{\alpha_s}{\pi} \Gamma(1 + \epsilon) (4\pi)^\epsilon \left\{ \frac{1}{\epsilon} + \log \frac{\bar{\mu}^2}{Q_0^2} \right\} \left\{ M_{\tilde{g}}^2 \mp M_{\tilde{g}}m_Q \sin 2\tilde{\theta}_Q \right\} \\
&\quad + \frac{\delta m_Q}{m_Q} \left\{ 2m_Q^2 \mp \frac{1}{2}(m_{\tilde{Q}_2}^2 - m_{\tilde{Q}_1}^2) \sin^2 2\tilde{\theta}_Q \right\}, \tag{31}
\end{aligned}$$

using the tree-level mixing angle $\tilde{\theta}_Q$ of Eq. (27), and $C_F = 4/3$. The counterterms of the parameters $\overline{M}_{\tilde{Q}_{L/R}}^2(Q_0)$ and $\overline{A}_Q(Q_0)$ are defined in the $\overline{\text{MS}}$ scheme,

$$\begin{aligned}\delta\overline{M}_{\tilde{Q}_{L/R}}^2 &= -C_F\frac{\alpha_s}{\pi}\Gamma(1+\epsilon)(4\pi)^\epsilon M_{\tilde{g}}^2\left\{\frac{1}{\epsilon}+\log\frac{\bar{\mu}^2}{Q_0^2}\right\} \\ \delta\overline{A}_Q &= C_F\frac{\alpha_s}{\pi}\Gamma(1+\epsilon)(4\pi)^\epsilon M_{\tilde{g}}\left\{\frac{1}{\epsilon}+\log\frac{\bar{\mu}^2}{Q_0^2}\right\}.\end{aligned}\quad (32)$$

The counterterm of the pole quark mass m_q is given by

$$\begin{aligned}\frac{\delta m_Q}{m_Q} &= -C_F\frac{\alpha_s}{4\pi}\left\{\frac{A_0(m_Q)}{m_Q^2}+2B_0(m_Q^2;0,m_Q)-1+B_1(m_Q^2;M_{\tilde{g}},m_{\tilde{Q}_1})+B_1(m_Q^2;M_{\tilde{g}},m_{\tilde{Q}_2})\right. \\ &\quad \left.+\delta_{SUSY}+2M_{\tilde{g}}(A_Q-\mu r_Q)\frac{B_0(m_Q^2;M_{\tilde{g}},m_{\tilde{Q}_1})-B_0(m_Q^2;M_{\tilde{g}},m_{\tilde{Q}_2})}{m_{\tilde{Q}_1}^2-m_{\tilde{Q}_2}^2}\right\},\end{aligned}\quad (33)$$

where $\delta_{SUSY} = 1/3$ is a finite counterterm required to restore the supersymmetric relation between the Higgs-boson couplings to quarks and squarks within dimensional regularization [40]. The definition of the mixing angle $\tilde{\theta}_Q$ in Eq. (27) corresponds to the following counterterm at NLO,

$$\begin{aligned}\delta\tilde{\theta}_Q &= \frac{\text{tg } 2\tilde{\theta}_Q}{2}\left\{\frac{\delta m_Q}{m_Q}+\frac{\delta\overline{A}_Q}{\overline{A}_Q(Q_0)-\mu r_Q}-\frac{\delta m_{\tilde{Q}_1}^2-\delta m_{\tilde{Q}_2}^2}{m_{\tilde{Q}_1}^2-m_{\tilde{Q}_2}^2}\right\}, \\ \delta m_{\tilde{Q}_{1/2}}^2 &= -\Sigma_{11/22}(m_{\tilde{Q}_{1/2}}^2).\end{aligned}\quad (34)$$

However, this mixing angle definition induces artificial singularities in physical observables for stop/sbottom masses $m_{\tilde{q}_{1,2}}$ close to each other [41]. To avoid such singularities, the mixing angle of the squark fields has been renormalized via the anti-Hermitian (on-shell) counterterm [41],

$$\delta\theta_Q = -\frac{1}{2}\frac{\text{Re } \Sigma_{12}(m_{\tilde{Q}_1}^2) - \text{Re } \Sigma_{12}(m_{\tilde{Q}_2}^2)}{m_{\tilde{Q}_1}^2 - m_{\tilde{Q}_2}^2},\quad (35)$$

with the off-diagonal part Σ_{12} of the stop/sbottom self-energy (see Fig. 4) describing transitions from the first to the second mass eigenstate or *vice versa*,

$$\Sigma_{12}(m^2) = -C_F\frac{\alpha_s}{\pi}\left\{M_{\tilde{g}}m_ QB_0(m^2;M_{\tilde{g}},m_Q)+\frac{\sin 2\tilde{\theta}_Q}{4}\left[A_0(m_{\tilde{Q}_2})-A_0(m_{\tilde{Q}_1})\right]\right\}\cos 2\tilde{\theta}_Q.\quad (36)$$

For the mixing angle $\tilde{\theta}_Q$ of Eq. (27), this implies a finite shift $\Delta\tilde{\theta}_Q$,

$$\theta_Q = \tilde{\theta}_Q + \Delta\tilde{\theta}_Q \quad , \quad \Delta\tilde{\theta}_Q = \delta\tilde{\theta}_Q - \delta\theta_Q\quad (37)$$

that will be absorbed in the shifted A_Q value of Eq. (26). This shift defines the relation between the on-shell coupling A_Q and the $\overline{\text{MS}}$ one $\overline{A}_Q(Q_0)$.

Using the NLO corrected squark pole masses of Eq. (28) and the radiatively corrected mixing angle θ_q , the shifted (on-shell) squared soft SUSY-breaking squark mass parameters $\tilde{M}_{\tilde{Q}_{L/R}}^2 = \tilde{M}_{\tilde{Q}_{L/R}}^2(Q_0) + \Delta\overline{M}_{\tilde{Q}_{L/R}}^2$ can be obtained from the sum rules,

$$\begin{aligned}\tilde{M}_{\tilde{Q}_L}^2 &= M_{\tilde{Q}_L}^2 + D_{\tilde{Q}_L} = m_{\tilde{Q}_1}^2 \cos^2 \theta_Q + m_{\tilde{Q}_2}^2 \sin^2 \theta_Q - m_Q^2 \\ \tilde{M}_{\tilde{Q}_R}^2 &= M_{\tilde{Q}_R}^2 + D_{\tilde{Q}_R} = m_{\tilde{Q}_1}^2 \sin^2 \theta_Q + m_{\tilde{Q}_2}^2 \cos^2 \theta_Q - m_Q^2\end{aligned}\quad (38)$$

while the shifted (on-shell) trilinear couplings A_Q are derived from the relation

$$A_Q = \frac{m_{\tilde{Q}_1}^2 - m_{\tilde{Q}_2}^2}{2m_Q} \sin 2\theta_Q + \mu r_Q. \quad (39)$$

In terms of these shifted (on-shell) parameters the radiatively corrected squark masses and mixing angles are given by LO-like expressions,

$$\begin{aligned}m_{\tilde{Q}_{1/2}}^2 &= m_Q^2 + \frac{1}{2} \left[\tilde{M}_{\tilde{Q}_L}^2 + \tilde{M}_{\tilde{Q}_R}^2 \mp \sqrt{(\tilde{M}_{\tilde{Q}_L}^2 - \tilde{M}_{\tilde{Q}_R}^2)^2 + 4m_Q^2(A_Q - \mu r_Q)^2} \right] \\ \sin 2\theta_Q &= \frac{2m_Q(A_Q - \mu r_Q)}{m_{\tilde{Q}_1}^2 - m_{\tilde{Q}_2}^2}, \quad \cos 2\theta_Q = \frac{\tilde{M}_{\tilde{Q}_L}^2 - \tilde{M}_{\tilde{Q}_R}^2}{m_{\tilde{Q}_1}^2 - m_{\tilde{Q}_2}^2}.\end{aligned}\quad (40)$$

The scale of the strong coupling constants α_s in Eqs. (29, 31, 32, 33, 36) has been identified with the input scale Q_0 .

These relations have been used for the determination of the $\overline{\text{MS}}$ parameters $\tilde{M}_{\tilde{Q}_{L/R}}^2(Q_0)$ and $\overline{A}_q(Q_0)$ iteratively until the on-shell parameters agreed with the input value of the chosen benchmark scenario.

4.2.2 Sbottoms

The procedure described for the stops is necessary to obtain the $\overline{\text{MS}}$ parameter $\overline{M}_{\tilde{t}_L}(Q_0)$ that by virtue of the SU(2) gauge symmetry is identified with the $\overline{\text{MS}}$ parameter $\overline{M}_{\tilde{b}_L}(Q_0)$,

$$\overline{M}_{\tilde{t}_L}(Q_0) = \overline{M}_{\tilde{b}_L}(Q_0). \quad (41)$$

Due to potentially large $\text{tg}\beta$ -enhanced contributions in the sbottom sector the procedure has to be modified. This modification addresses the treatment and renormalization of the bottom mass m_b and of the trilinear coupling A_b . Therefore, the bottom mass is not introduced as the pole mass, but as a derived quantity, since it represents the contribution of the bottom Yukawa coupling to the sbottom sector. To achieve a working scheme, we are starting from Eq. (40) for the mixing angle that at NLO is still defined via the anti-Hermitian counterterm of Eq. (35). The trilinear coupling A_b , however, is now defined from the proper $A\tilde{b}_1\tilde{b}_2$ vertex [38]. This definition avoids large $\text{tg}\beta$ -enhanced contributions in the renormalization

of A_b . The bottom mass m_b entering the sbottom mixing matrix is then treated as a derived quantity. This leads to the explicit counterterms,

$$\begin{aligned}\delta A_b &= -\frac{s_{\beta}c_{\beta}}{\mu}(A_b - \mu t g \beta) \left(A_b + \frac{\mu}{t g \beta} \right) \left\{ F - 2\frac{c_{2\theta_b}}{s_{2\theta_b}}\delta\theta_b - \frac{\delta m_{\tilde{b}_1}^2 - \delta m_{\tilde{b}_2}^2}{m_{\tilde{b}_1}^2 - m_{\tilde{b}_2}^2} \right\} \\ \frac{\delta \hat{m}_b}{m_b} &= \left\{ 1 + \frac{s_{\beta}c_{\beta}}{\mu}(A_b - \mu t g \beta) \right\} F - \frac{s_{\beta}c_{\beta}}{\mu}(A_b - \mu t g \beta) \left\{ 2\frac{c_{2\theta_b}}{s_{2\theta_b}}\delta\theta_b + \frac{\delta m_{\tilde{b}_1}^2 - \delta m_{\tilde{b}_2}^2}{m_{\tilde{b}_1}^2 - m_{\tilde{b}_2}^2} \right\},\end{aligned}\quad (42)$$

where the term F is defined as [42]

$$\begin{aligned}F &= f(m_{\tilde{b}_1}^2, m_{\tilde{b}_2}^2) + f(m_{\tilde{b}_2}^2, m_{\tilde{b}_1}^2) \\ f(m_1^2, m_2^2) &= -\frac{C_F}{2} \frac{\alpha_s}{\pi} \left\{ -\frac{M_{\tilde{g}}}{A_b + \mu \cot \beta} B_0(m_1^2; M_{\tilde{g}}, m_b) \right. \\ &\quad \left. + \frac{m_1^2}{m_1^2 - m_2^2} \left[2B_0(m_1^2; 0, m_1) - \frac{m_1^2 - M_{\tilde{g}}^2 - m_b^2}{m_1^2} B_0(m_1^2; M_{\tilde{g}}, m_b) \right] \right\}.\end{aligned}\quad (43)$$

The derived bottom mass \hat{m}_b is then determined as

$$\hat{m}_b = \overline{m}_b(Q_0) - \delta \hat{m}_b + \delta \overline{m}_b, \quad (44)$$

where $\overline{m}_b(Q_0)$ denotes the $\overline{\text{MS}}$ bottom mass at the input scale Q_0 , $\delta \hat{m}_b$ the counterterm of Eq. (42) and $\delta \overline{m}_b$ the $\overline{\text{MS}}$ counterterm of the bottom mass,

$$\begin{aligned}\frac{\delta \overline{m}_b}{m_b} &= -C_F \frac{\alpha_s}{\pi} \Gamma(1 + \epsilon) (4\pi)^\epsilon \frac{3}{4} \left\{ \frac{1}{\epsilon} + \log \frac{\overline{\mu}^2}{Q_0^2} + \delta_{SUSY} \right\} \\ &\quad - C_F \frac{\alpha_s}{4\pi} \left\{ B_1[m_b^2; M_{\tilde{g}}, m_{\tilde{b}_1}] + B_1[m_b^2; M_{\tilde{g}}, m_{\tilde{b}_2}] \right. \\ &\quad \left. + 2M_{\tilde{g}}(A_b - \mu t g \beta) \frac{B_0[m_b^2; M_{\tilde{g}}, m_{\tilde{b}_1}] - B_0[m_b^2; M_{\tilde{g}}, m_{\tilde{b}_2}]}{m_{\tilde{b}_1}^2 - m_{\tilde{b}_2}^2} \right\},\end{aligned}\quad (45)$$

where $\delta_{SUSY} = 1/3$ is a SUSY-restoring counterterm. This $\overline{\text{MS}}$ counterterm defines the running bottom mass with decoupled SUSY contributions, i.e. the running bottom mass of the SM. The derived bottom mass \hat{m}_b is then used for the sbottom mixing matrix throughout. In the analogous way we determine the $\overline{\text{MS}}$ value $\overline{A}_b(Q_0)$ of the trilinear coupling, but this will not be used in our analysis.

The shifted (on-shell) sbottom mass parameters $\tilde{M}_{\tilde{b}_{L/R}}$ are finally determined from the corresponding sum rules of Eq. (38). This set-up of the sbottom sector is then used for iteration until the on-shell parameter $\tilde{M}_{\tilde{b}_R}$ agrees with the input parameter of the benchmark scenario.

An alternative approach is provided by a purely fixed-order implementation of the difference between $M_{\tilde{b}_L}$ and $M_{\tilde{t}_L}$,

$$\begin{aligned}M_{\tilde{b}_L}^2 &= M_{\tilde{t}_L}^2 + \Delta M_L^2 \\ \Delta M_L^2 &= \delta M_{\tilde{t}_L}^2 - \delta M_{\tilde{b}_L}^2 \\ \delta M_{\tilde{q}_L}^2 &= c_{\theta_q}^2 \delta m_{\tilde{q}_1}^2 + s_{\theta_q}^2 \delta m_{\tilde{q}_2}^2 - (m_{\tilde{q}_1}^2 - m_{\tilde{q}_2}^2) s_{2\theta_q} \delta \theta_q - 2m_q \delta m_q,\end{aligned}\quad (46)$$

with $q = t, b$. The counterterms $\delta m_{\tilde{q}_{1/2}}$ are given in Eq. (34), the counterterm $\delta\theta_q$ in Eq. (35) and the counterterm δm_q in Eq. (33) for the top pole mass $m_q = m_t$ and in Eq. (42) for the (derived) bottom mass $m_q = \hat{m}_b$. This approach does not require any iteration, since the on-shell parameters of the benchmark scenario can immediately be used to derive the parameters of the sbottom sector. We have compared both approaches and found agreement of the sbottom parameters at the few-per-mille level.

4.2.3 Higgs Couplings to Stops and Sbottoms

The NLO neutral Higgs couplings to squarks in the current-eigenstate basis are given by

$$\begin{aligned} g_{\tilde{Q}_L\tilde{Q}_L}^\Phi &= m_Q^2 g_1^\Phi + M_Z^2 (I_{3Q} - e_Q \sin^2 \theta_W) g_2^\Phi \\ g_{\tilde{Q}_R\tilde{Q}_R}^\Phi &= m_Q^2 g_1^\Phi + M_Z^2 e_Q \sin^2 \theta_W g_2^\Phi \\ g_{\tilde{Q}_L\tilde{Q}_R}^\Phi &= \frac{m_Q}{2} [\mu g_3^\Phi - A_Q g_4^\Phi] , \end{aligned} \quad (47)$$

with the on-shell trilinear couplings A_Q and the couplings g_i^Φ of Table 1. The quark mass m_Q denotes either the top pole mass in the stop case or the derived bottom mass \hat{m}_b for the sbottom sector. The related couplings to the stop/sbottom mass eigenstates $\tilde{Q}_{1,2}$ are derived by the rotations according to Eq. (22) by the radiatively corrected mixing angle θ_Q . For pseudoscalar Higgs bosons, we obtain vanishing diagonal couplings $g_{\tilde{Q}_L\tilde{Q}_L}^A = g_{\tilde{Q}_R\tilde{Q}_R}^A = 0$ and non-vanishing off-diagonal couplings $g_{\tilde{Q}_1\tilde{Q}_2}^A = -g_{\tilde{Q}_2\tilde{Q}_1}^A = g_{\tilde{Q}_L\tilde{Q}_R}^A$ at the NLO level as at LO.

5 SUSY–QCD corrections at NLO

The genuine SUSY–QCD corrections at NLO are determined by the Feynman diagrams shown in Fig. 5 that displays only the non-vanishing graphs. Additional permutations of the external gluons have to be added. The matrix element for the LO expression and the SUSY–QCD corrections can be parametrized as

$$\begin{aligned} \mathcal{M} &= i\delta_{ab} \frac{\alpha_s}{2\pi v} \mathcal{T}^{\mu\nu} \epsilon_\mu(q_1) \epsilon_\nu(q_2) \\ \mathcal{T}^{\mu\nu} &= A_{LO/SQCD}^A \epsilon^{\mu\nu\alpha\beta} q_{1\alpha} q_{2\beta} , \end{aligned} \quad (48)$$

where q_1, q_2 denote the two incoming momenta of the gluons and $\epsilon_\mu(q_i)$ their polarization vectors, δ_{ab} the Kronecker symbol of the adjoint $SU(3)_c$ color space and $\epsilon^{\mu\nu\alpha\beta}$ the four-dimensional Levi–Civita tensor. In this paper we will mainly use the γ_5 prescription of Larin [27], where the product of Levi–Civita tensors is replaced by the determinant of n -dimensional metric tensors in $n = 4 - 2\epsilon$ dimensions. Within this framework we can construct a projector on the anticipated form factors $A_{LO/SQCD}^A$,

$$\mathcal{P}^{\mu\nu} = \frac{2}{M_A^4 (1 - \epsilon)(1 - 2\epsilon)} \epsilon^{\mu\nu\alpha\beta} q_{1\alpha} q_{2\beta} \quad (49)$$

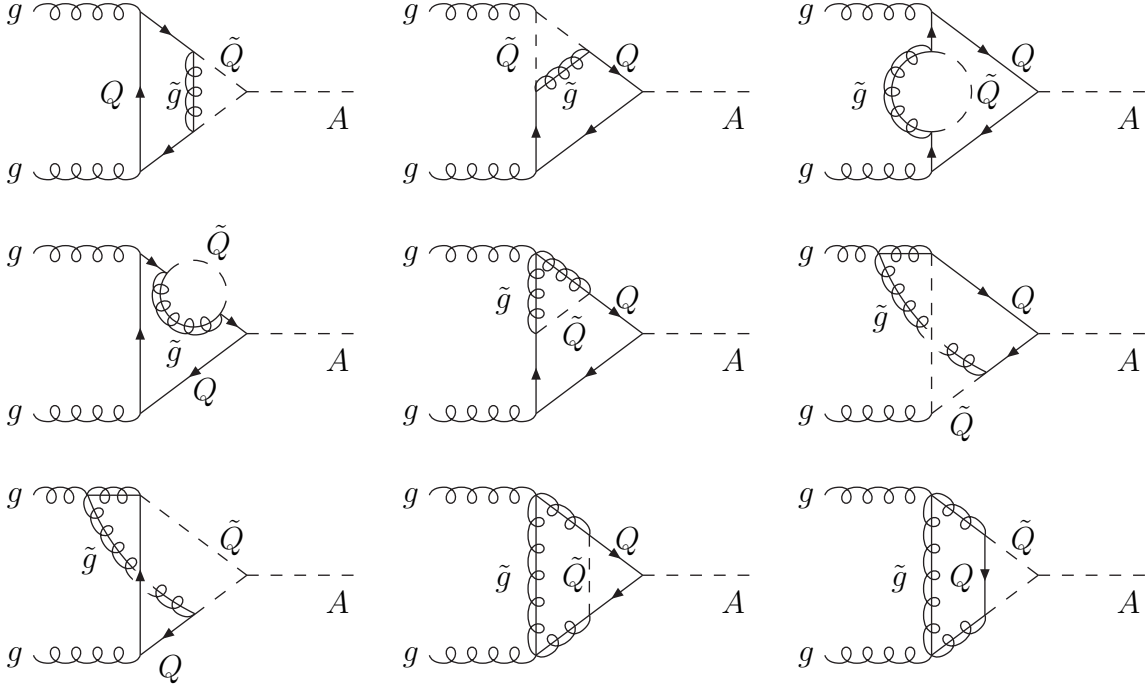


Figure 5: *Non-vanishing diagrams contributing to the genuine SUSY-QCD corrections to pseudoscalar MSSM Higgs boson production via gluon fusion mediated by top- and bottom quark ($Q = t, b$) as well as stop/sbottom ($\tilde{Q} = \tilde{t}, \tilde{b}$) and gluino (\tilde{g}) loops at NLO.*

so that

$$\mathcal{P}^{\mu\nu}\mathcal{T}_{\mu\nu} = A_{LO/SQCD}^A . \quad (50)$$

In order to set up a simple notation in close connection to the QCD corrections of Eq. (5) we will normalize the genuine SUSY-QCD corrections to the individual form factors at LO,

$$A_{Q,SQCD}^A = A_{Q,LO}^A \mathcal{C}_{Q,SQCD}^A \frac{\alpha_s}{\pi} , \quad (51)$$

where $\mathcal{C}_{Q,SQCD}^A$ depends on all ratios of the pseudoscalar Higgs, quark, squark and gluino masses. The LO form factor

$$A_{Q,LO}^A = \Gamma(1 + \epsilon) \left(\frac{4\pi\bar{\mu}^2}{m_Q^2} \right)^\epsilon m_Q g_Q^A A_Q^A(\tau_Q) \quad (52)$$

has been defined in terms of the expressions of Eq. (2). In the following we will describe the technical details for the numerical integration to determine the complex coefficient $\mathcal{C}_{Q,SQCD}$ by exemplifying our method for the first diagram of Fig. 5. In order to regularize virtual

thresholds we have added a small imaginary part to the quark and squark masses²,

$$m_Q^2 \rightarrow m_Q^2(1 - i\bar{\epsilon}), \quad m_{\tilde{Q}_k}^2 \rightarrow m_{\tilde{Q}_k}^2(1 - i\bar{\epsilon}) \quad (k = 1, 2), \quad (53)$$

with a positive regulator $\bar{\epsilon} > 0$, which defines the analytical continuation of our two-loop amplitudes. We work with a small but finite value of $\bar{\epsilon}$ that is small enough to achieve results in the narrow-width approximation. For the parametrization of the two-loop diagrams, we follow the same procedure used and described in Refs. [43] for Higgs-boson pair production and adopted in earlier works [44].

5.1 Feynman Parametrization

The parametrization of the first two-loop diagram of Fig. 5 reads

$$\begin{aligned} \mathcal{T}_1^{\mu\nu} &= -\frac{C_F}{4} \frac{g_{\tilde{Q}_l\tilde{Q}_m}^A}{m_Q} \frac{\alpha_s}{\pi} (4\pi)^4 A_{1,lm}^{\mu\nu} \\ A_{1,lm}^{\mu\nu} &= \int \frac{d^n k d^n q}{(2\pi)^{2n}} \frac{\text{Tr} \left\{ \overline{\mathcal{P}}_l(-\not{q} + M_{\tilde{g}}) \mathcal{P}_m(\not{k} + \not{q}_1 + m_Q) \gamma^\mu (\not{k} + m_Q) \gamma^\nu (\not{k} - \not{q}_2 + m_Q) \right\}}{(k^2 - m_Q^2)[(k + q_1)^2 - m_Q^2][(k - q_2)^2 - m_Q^2][(k + q + q_1)^2 - m_{\tilde{Q}_m}^2]} \\ &\quad \times \frac{1}{[(k + q - q_2)^2 - m_{\tilde{Q}_l}^2](q^2 - M_{\tilde{g}}^2)} \end{aligned} \quad (54)$$

where we sum over $l, m \in \{1, 2\}$ in $\mathcal{T}_1^{\mu\nu}$, k, q are the loop momenta that are integrated over and the chiral coupling factors \mathcal{P}_j ($j = 1, 2$) are defined as

$$\begin{aligned} \mathcal{P}_1 &= \mathcal{P}_L \cos \theta_Q - \mathcal{P}_R \sin \theta_Q \\ \mathcal{P}_2 &= -\mathcal{P}_L \sin \theta_Q - \mathcal{P}_R \cos \theta_Q \\ \mathcal{P}_{R/L} &= \frac{1 \pm \gamma_5}{2}, \end{aligned} \quad (55)$$

and $\overline{\mathcal{P}}_j$ emerges from \mathcal{P}_j by the replacement $\gamma_5 \rightarrow -\gamma_5$. After applying the contraction with the projector $\mathcal{P}_{\mu\nu}$ onto the contribution to the virtual form factor, we introduce Feynman parameters x_3, x_4, x_1, x_2 for the second to fifth propagator (in this ordering) and $1 - \sum_j x_j$ for the first one, $(k^2 - m_Q^2)$. With the substitutions

$$x_1 = (1 - x)y, \quad x_2 = (1 - x)(1 - y), \quad x_3 = x(1 - z), \quad x_4 = xzv \quad (56)$$

we obtain a four-dimensional Feynman-parameter integral over x, y, z, v with integration boundaries from 0 to 1. The shift

$$\begin{aligned} k &\rightarrow k - Q_1 \\ Q_1 &= (1 - x)q + [x + y - x(y + z)]q_1 - [(1 - x)(1 - y) + xzv]q_2 \end{aligned} \quad (57)$$

²This procedure is equivalent to adding an imaginary part to the gluino mass in addition, but in our numerical analysis we do not cross virtual thresholds involving the gluino so that this addition is not required.

in both the numerator and denominator symmetrizes the k -integration that is performed in a simple and systematic way for the emerging integral. The residual q -dependent denominator after the k -integration is treated as a propagator for the q -integration after extracting all coefficients in front of the term q^2 . We introduce a fifth Feynman parameter r for this propagator and $1 - r$ for the last purely q^2 -dependent propagator of Eq. (54). Applying the second shift

$$\begin{aligned} q &\rightarrow q - Q_2, \\ Q_2 &= -r(1 - y - z)q_1 - r(1 - y - zv)q_2 \end{aligned} \quad (58)$$

both in the numerator and denominator we perform the symmetric q -integration. In this way, we finally arrive at an integral of the type

$$A_{1,SQCD}^A = \frac{C_F g_{\tilde{Q}_l \tilde{Q}_m}^A}{4 m_Q} \frac{\alpha_s}{\pi} \Gamma(2 + 2\epsilon) \left(\frac{4\pi\mu_0^2}{M_{\tilde{g}}^2} \right)^{2\epsilon} \int_0^1 d^5x \frac{x^{1+\epsilon}(1-x)^\epsilon z r^{2+\epsilon} H(\vec{x})}{N^{2+2\epsilon}(\vec{x})}, \quad (59)$$

with $\vec{x} = (x, y, z, v, r)$ and $d^5x = dx dy dz dv dr$. The term $H(\vec{x})$ denotes the full numerator and includes singular and higher powers of the dimensional regulator ϵ . $N(\vec{x})$ is the final denominator,

$$\begin{aligned} N(\vec{x}) &= x(1-x)(1-r) + \rho_Q x r + \rho_m (1-x) y r + \rho_l (1-x)(1-y)r \\ &+ \rho_A r \left\{ x(1-x)r(1-y-z)(1-y-zv) \right. \\ &\quad \left. - [y(1-x) + x(1-z)][(1-x)(1-y) + xzv] \right\} \end{aligned} \quad (60)$$

where the ratios are defined as $\rho_Q = m_Q^2/M_{\tilde{g}}^2$, $\rho_k = m_{\tilde{Q}_k}^2/M_{\tilde{g}}^2$, $\rho_A = M_A^2/M_{\tilde{g}}^2$. This denominator is maximally a second-order polynomial in all Feynman parameters we have introduced. The poles of $H(\vec{x})$ in ϵ originate from powers of k^2 and q^2 in the numerators of the k - and q -integrals. We have chosen the convention to normalize all mass parameters to the gluino mass $M_{\tilde{g}}$. In order to cope with the LO form factor in an easier way, we have rewritten the coefficients of all integrals as

$$\Gamma(2 + 2\epsilon) \left(\frac{4\pi\mu_0^2}{M_{\tilde{g}}^2} \right)^{2\epsilon} = \Gamma^2(1 + \epsilon) \left(\frac{4\pi\mu_0^2}{m_Q^2} \right)^\epsilon \left(\frac{4\pi\mu_0^2}{M_{\tilde{g}}^2} \right)^\epsilon \times \rho_Q^\epsilon (1 + 2\epsilon)(1 + \epsilon^2 \zeta_2) + \mathcal{O}(\epsilon^3). \quad (61)$$

The factors $\rho_Q^\epsilon (1 + 2\epsilon)(1 + \epsilon^2 \zeta_2)$ are added to the integrands before expansion in ϵ . The final contribution to the coefficient $\mathcal{C}_{Q,SQCD}^A$ is then given by

$$\begin{aligned} \mathcal{C}_{Q,SQCD}^{A,(1)} &= \frac{C_F}{4} \frac{g_{\tilde{Q}_l \tilde{Q}_m}^A}{m_Q^2 g_{\tilde{Q}^A \tilde{Q}^A}^A(\tau_Q)} \Gamma(1 + \epsilon) \left(\frac{4\pi\mu_0^2}{M_{\tilde{g}}^2} \right)^\epsilon \int_0^1 d^5x \frac{x^{1+\epsilon}(1-x)^\epsilon z r^{2+\epsilon} H(\vec{x})}{N^{2+2\epsilon}(\vec{x})} \\ &\quad \times \rho_Q^\epsilon (1 + 2\epsilon + \epsilon^2 \zeta_2). \end{aligned} \quad (62)$$

The final integral is finite for this diagram. For the other diagrams, we follow the same procedure accordingly. All diagrams are infrared finite, since all virtual particles are massive, but the residual Feynman integrals contain end-point singularities in several cases that are subtracted in the usual way according to the description of Ref. [43]. The integration of the subtracted part yields the corresponding UV singularities.

5.2 Integration by Parts

In our numerical analysis, we cross the virtual $b\bar{b}, t\bar{t}$ thresholds and for large pseudoscalar masses the $\tilde{b}_1\tilde{b}_2^*, \tilde{t}_1\tilde{t}_2^*$ thresholds as well. The parametrization of the integrals discussed so far is not sufficiently stable above these thresholds due to the high power of the denominator $N(\vec{x})$ that becomes small in the Feynman-parameter regions in the vicinity of the virtual thresholds. We need to adopt imaginary regulators $\bar{\varepsilon} \lesssim 10^{-3}$ in order to obtain numbers independent of this regulator. The small size of this regulator makes the integral numerically unstable. A stabilization of the integration can be achieved by an integration by parts (IBP) to reduce the power of the denominator. In general, for this purpose, one can write

$$\Delta = p_0 N + \sum_i p_i \frac{\partial N}{\partial x_i} \quad (63)$$

where N is the dominator of the integral, p_0 and p_i are polynomials and Δ is constant in the variables x_i . For simplicity we drop the arguments \vec{x} everywhere. The polynomials p_0 and p_i can be found by constructing the Gröbner basis of the set $\{N, \frac{\partial N}{\partial x_i}\}$. We find that

$$\begin{aligned} \int_0^1 d^n x \frac{g_m}{N^{m+2\varepsilon}} &= \int_0^1 d^n x \frac{g_{m-1}}{N^{m-1+2\varepsilon}} + \sum_i \left[\frac{g_{m-1}^{(i)}}{N^{m-1+2\varepsilon}} \right]_{x_i=0}^{x_i=1} \\ g_{m-1} &= \frac{1}{\Delta} \left(g_m p_0 - \frac{\sum_i \partial_{x_i} (g_m p_i)}{1 - m - 2\varepsilon} \right) \\ g_{m-1}^{(i)} &= \frac{1}{\Delta} \frac{g_m p_i}{1 - m - 2\varepsilon}. \end{aligned} \quad (64)$$

These equations can be applied iteratively to reduce the power of the denominator further. Not every choice of the parameters for the integration by parts will yield a stable result. Potential issues can arise from singularities in the boundary terms as well as singularities that arise when $\Delta = 0$, which can happen when $N = 0$ and all $\frac{\partial N}{\partial x_i} = 0$.

Choosing only a subset of the Feynman parameters yields shorter expressions that can be evaluated faster. For practical purposes, it is thus usually best to find a parametrization where using a single Feynman parameter for the integration by parts is sufficient to stabilize the numerical integration.

We exemplify the two examples encountered in our calculation. If N is linear in the Feynman parameter x_1 , i.e.

$$N = ax_1 + b, \quad (65)$$

there are two possible choices for the polynomials

$$p_0 = 0 \quad p_1 = 1 \quad \Delta = a \quad (66)$$

$$\text{or } p_0 = 1 \quad p_1 = -x_1 \quad \Delta = b. \quad (67)$$

A linear combination of these two solutions is also valid. If N is quadratic in the Feynman parameter i.e.

$$N = ax_1^2 + bx_1 + c, \quad (68)$$

the polynomials are given by

$$p_0 = 4a \qquad p_1 = -b - 2ax_1 \qquad \Delta = -b^2 + 4ac. \quad (69)$$

For example in the first diagram we have achieved stabilization for $x_1 = v$. The denominator is linear in this parameter and we have

$$\begin{aligned} N(\vec{x}) &= av + b \\ a &= -\rho_A xzr \left\{ r(1-z) + (1-r)[y(1-x) + x(1-z)] \right\} \\ b &= x(1-x)(1-r) + \rho_Q xr + \rho_m(1-x)yr + \rho_l(1-x)(1-y)r \\ &\quad + \rho_A(1-x)(1-y)r \left\{ xr(1-y-z) - [y(1-x) + x(1-z)] \right\}. \end{aligned} \quad (70)$$

With this explicit parametrization at hand, the following manipulation can be performed,

$$\begin{aligned} \int_0^1 dv \frac{H_i(\vec{x})}{N^2(\vec{x})} &= \frac{H(\vec{x})|_{v=0}}{ab} - \frac{H(\vec{x})|_{v=1}}{a(a+b)} + \frac{[\partial_v H(\vec{x})]|_{v=1} \log(a+b) - [\partial_v H(\vec{x})]|_{v=0} \log(b)}{a^2} \\ &\quad - \int_0^1 \frac{dv}{a^2} [\partial_v^2 H(\vec{x})] \log(av+b), \end{aligned} \quad (71)$$

according to Eq. (64). Since the powers of all denominators are reduced and the original denominator $N(\vec{x})$ appears in the argument of a logarithm in the last integral the numerical integration appears to be stable for the imaginary regulator down to $\bar{\epsilon} \lesssim 10^{-4}$ which is sufficient for the narrow-width limit.

In cases of a Feynman parameter entering the denominator in second order,

$$N(\vec{x}) = ay^2 + by + c \quad (72)$$

and making use of the identities of Eq. (69) (we drop the arguments of N)

$$\Delta = 4ac - b^2 = 4aN - (\partial_y N)^2 = 4aN - (2ay + b)^2, \quad (73)$$

we arrive at the special situation that the derivative appears in second power. This allows us to perform two IBPs of the original integral [43],

$$\int_0^1 dy \frac{H}{N^2} = \frac{1}{\Delta} \left\{ \left[\frac{2ay+b}{N} H - (\partial_y H) \log N \right] \Big|_{y=0}^{y=1} + \int_0^1 dy \left[\frac{2a}{N} H + (\partial_y^2 H) \log N \right] \right\}, \quad (74)$$

where for simplicity we dropped the arguments \vec{x} everywhere.

5.3 Renormalization

In our calculation of the genuine SUSY-QCD corrections we have to renormalize the SUSY-QCD part of the quark mass only, since everything else is already accounted for by the QCD corrections, i.e. the decoupling of all SUSY particles from the evolution of the strong

coupling α_s and the PDFs that both run with five active flavours in our calculation. The SUSY-QCD part of the on-shell quark-mass counterterm is given by [see Eq. (33)]

$$\begin{aligned} \frac{\delta m_Q}{m_Q} = & -C_F \frac{\alpha_s}{4\pi} \left\{ B_1(m_Q^2; M_{\tilde{g}}, m_{\tilde{Q}_1}) + B_1(m_Q^2; M_{\tilde{g}}, m_{\tilde{Q}_2}) \right. \\ & \left. + 2M_{\tilde{g}}(A_Q - \mu r_Q) \frac{B_0(m_Q^2; M_{\tilde{g}}, m_{\tilde{Q}_1}) - B_0(m_Q^2; M_{\tilde{g}}, m_{\tilde{Q}_2})}{m_{\tilde{Q}_1}^2 - m_{\tilde{Q}_2}^2} \right\}. \end{aligned} \quad (75)$$

We renormalize the quark mass on-shell, because the LO form factor $A_Q^A(\tau_Q)$ and the pure QCD corrections are expressed in terms of the quark pole mass³. The corresponding counterterm for the gluon-fusion cross section form factor is given by

$$\delta_1 A_{Q,SQCD}^A = \frac{\partial \tilde{A}_Q^A(\tau_Q)}{dm_Q} \delta m_Q = 2 \tau_Q \frac{\partial \tilde{A}_Q^A(\tau_Q)}{\partial \tau_Q} \frac{\delta m_Q}{m_Q}, \quad (76)$$

where $\tilde{A}_Q^A(\tau_Q)$ denotes the LO form factor including $\mathcal{O}(\epsilon)$ terms,

$$\begin{aligned} \tilde{A}_Q^A(\tau) &= \tau f(\tau) + \epsilon \frac{\tau}{4} H(\tau) + \mathcal{O}(\epsilon^2) \\ H(\tau) &= 4 \left\{ S_{1,2}(x) + S_{1,2}\left(\frac{1}{x}\right) \right\} + 2 \left\{ Li_3(x) + Li_3\left(\frac{1}{x}\right) \right\} + 2\zeta_3 \\ x &= \frac{1 - \sqrt{1 - \tau}}{1 + \sqrt{1 - \tau}}, \end{aligned} \quad (77)$$

with the usual trilogarithms,

$$\begin{aligned} S_{1,2}(y) &= \frac{1}{2} \int_0^1 \frac{dz}{z} \log^2(1 - zy) \\ Li_3(y) &= \int_0^1 \frac{dz}{z} \log(z) \log(1 - zy). \end{aligned} \quad (78)$$

The derivative is given by

$$\begin{aligned} \tau \frac{\partial \tilde{A}_Q^A(\tau)}{\partial \tau} &= \tilde{A}_Q^A(\tau) + \frac{\tau}{1 - \tau} g(\tau) + \frac{\epsilon}{2} \left\{ \frac{\tau}{\tau - 1} g(\tau) \log\left(4 \frac{\tau - 1}{\tau}\right) \right. \\ &\quad \left. + \frac{\tau}{\sqrt{1 - \tau}} \left[Li_2\left(\frac{1}{1 - x}\right) - Li_2\left(\frac{-x}{1 - x}\right) \right] \right\} \\ g(\tau) &= \begin{cases} \sqrt{\tau - 1} \arcsin \frac{1}{\sqrt{\tau}} & \tau \geq 1 \\ \frac{\sqrt{1 - \tau}}{2} \left[\log \frac{1 + \sqrt{1 - \tau}}{1 - \sqrt{1 - \tau}} - i\pi \right] & \tau < 1 \end{cases} \end{aligned} \quad (79)$$

³For the evaluation of the NLO SUSY-QCD contributions, however, we use the derived bottom mass \hat{m}_b [see Eq.(44)] in the calculation of $C_{b,SQCD}^A$. The resulting difference only contributes at the NNLO level.

where Li_2 denotes the dilogarithm,

$$Li_2(y) = - \int_0^1 \frac{dz}{z} \log(1 - zy) . \quad (80)$$

However, we introduce effective low-energy Yukawa couplings in our calculation, i.e. the Yukawa couplings of a low-energy Two-Higgs-Doublet model (2HDM), where the heavy SUSY particles are integrated out. This implies that the top- and bottom-Yukawa couplings are dressed with $\Delta_{t/b}$ contributions. The SUSY-QCD parts of these contributions are given by

$$\begin{aligned} \Delta_Q &= \frac{C_F}{2} \frac{\alpha_s(\mu_R)}{\pi} M_{\tilde{g}} \mu r_Q I(m_{\tilde{Q}_1}^2, m_{\tilde{Q}_2}^2, M_{\tilde{g}}^2) \\ I(a, b, c) &= \frac{ab \log \frac{a}{b} + bc \log \frac{b}{c} + ca \log \frac{c}{a}}{(a-b)(b-c)(a-c)} . \end{aligned} \quad (81)$$

The expressions for the Yukawa couplings including resummations of the leading $\cot \beta$ -enhanced contributions for the top-Yukawa coupling and the $\tan \beta$ -enhanced terms of the bottom Yukawa coupling can be cast into the form

$$g_Q^A \rightarrow \tilde{g}_Q^A = \frac{g_Q^A}{1 + \Delta_Q} \left[1 - \frac{\Delta_Q}{r_Q^2} \right] , \quad (82)$$

with r_Q defined after Eq. (17). These contributions will result in additional terms in the counterterms of our calculation,

$$\Delta A_{Q,SQCD}^A = A_Q^A(\tau_Q) \left(1 + \frac{1}{r_Q^2} \right) \Delta_Q , \quad (83)$$

since the LO form factors $A_Q^A(\tau_Q)$ are proportional to the *linear* quark-Yukawa coupling. This results in the complete counterterm

$$\delta A_{Q,SQCD}^A = 2 \tau_Q \frac{\partial \tilde{A}_Q^A(\tau_Q)}{\partial \tau_Q} \frac{\delta m_Q}{m_Q} + \Delta A_Q^A(\tau_Q) \quad (84)$$

5.4 Hadronic Cross Section

Our notation can be viewed as a modification of the factor σ_0^A of Eq. (1) as a starting point that can easily be extended to the NLO corrections,

$$\begin{aligned} \sigma_0^A &= \frac{G_F \alpha_s^2}{128 \sqrt{2} \pi} \left| g_t^A A_t(\tau_t) \left(1 + \hat{C}_{t,SQCD}^A \frac{\alpha_s}{\pi} \right) + g_b^A A_b(\tau_b) \left(1 + \hat{C}_{b,SQCD}^A \frac{\alpha_s}{\pi} \right) \right|^2 \\ &= \frac{G_F \alpha_s^2}{128 \sqrt{2} \pi} \left\{ |\tilde{g}_t^A A_t(\tau_t) + \tilde{g}_b^A A_b(\tau_b)|^2 \right. \\ &\quad \left. + 2 \operatorname{Re} \left[[\tilde{g}_t^A A_t(\tau_t) + \tilde{g}_b^A A_b(\tau_b)]^* [g_t^A A_t(\tau_t) \mathcal{C}_{t,SQCD}^A + g_b^A A_b(\tau_b) \mathcal{C}_{b,SQCD}^A] \frac{\alpha_s}{\pi} \right] + \mathcal{O}(\alpha_s^2) \right\} \end{aligned} \quad (85)$$

where \tilde{g}_Q^A ($Q = t, b$) denote the resummed quark Yukawa couplings of Eq. (82) that absorb Δ_b and Δ_t contributions in the effective Yukawa couplings as the appropriate effective Yukawa couplings in the low-energy effective 2HDM. The factors $\mathcal{C}_{Q,SQCD}^A$ and $\hat{\mathcal{C}}_{Q,SQCD}^A$ ($Q = t, b$) denote the relative SUSY–QCD corrections factors to the individual form factors with and without absorption of the Δ_Q terms, respectively. Within this framework the Yukawa couplings of the QCD corrections will be replaced by these effective Yukawa couplings as well due to the factorizing properties of EFT couplings from the pure QCD corrections. However, the subleading contributions of Eq. (85) involve the LO Yukawa couplings, since $\Delta_{t,b}$ effects only factorize at the leading order of an $1/M_{SUSY}^2$ expansion so that the SUSY–QCD remainder does not factorize from the effective Yukawa couplings in general. This will avoid artificial singularities in the scalar MSSM Higgs sector as well [45]. Expressing the LO factor σ_0^A in terms of the effective Yukawa couplings,

$$\sigma_0^A \rightarrow \tilde{\sigma}_0^A = \frac{G_F \alpha_s^2}{128 \sqrt{2} \pi} |\tilde{g}_t^A A_t(\tau_t) + \tilde{g}_b^A A_b(\tau_b)|^2, \quad (86)$$

and referring to Eq. (6), the SUSY–QCD corrections add to the virtual coefficient C^A ,

$$C^A = C_{QCD}^A + C_{SQCD}^A, \quad (87)$$

with the usual QCD-correction coefficient C_{QCD}^A and

$$C_{SQCD}^A = 2 \operatorname{Re} \left\{ \frac{g_t^A A_t(\tau_t) \mathcal{C}_{t,SQCD}^A + g_b^A A_b(\tau_b) \mathcal{C}_{b,SQCD}^A}{\tilde{g}_t^A A_t(\tau_t) + \tilde{g}_b^A A_b(\tau_b)} \right\}, \quad (88)$$

where we are using LO Yukawa couplings g_Q^A in the numerator, since this contribution constitutes the remainder of the full SUSY–QCD corrections that does not factorize in general terms. In Eq. (85) and for the following discussion of the results, we distinguish between this coefficient for the SUSY-remainder and the corresponding coefficient⁴,

$$\begin{aligned} \hat{C}_{SQCD}^A &= \bar{C}_{SQCD}^A - 2 \operatorname{Re} \left\{ \frac{g_t^A \Delta A_{t,SQCD} + g_b^A \Delta A_{b,SQCD}}{g_t^A A_t(\tau_t) + g_b^A A_b(\tau_b)} \right\} \\ \bar{C}_{SQCD}^A &= 2 \operatorname{Re} \left\{ \frac{g_t^A A_t(\tau_t) \mathcal{C}_{t,SQCD}^A + g_b^A A_b(\tau_b) \mathcal{C}_{b,SQCD}^A}{g_t^A A_t(\tau_t) + g_b^A A_b(\tau_b)} \right\} \end{aligned} \quad (89)$$

that describes the full SUSY–QCD corrections without introducing the effective top and bottom Yukawa couplings, i.e. without absorbing Δ_Q terms in the Yukawa couplings. The contributions $\Delta A_{Q,SQCD}$ are given in Eq. (83).

5.5 Axial γ_5 Schemes

We have implemented the Larin scheme of Ref. [27] that is a variant of the original 't Hooft–Veltman scheme that has been set-up systematically by Breitenlohner and Maison [26]. We

⁴Note that in the case of $\hat{C}_{Q,SQCD}^A$ we have to normalize to the LO expression with LO, i.e. *without* effective, Yukawa couplings.

have extracted the Levi–Civita tensor at the pseudoscalar vertex by means of the replacement

$$\gamma_5 = \frac{i}{24} \epsilon_{\mu\nu\rho\sigma} \gamma^\mu \gamma^\nu \gamma^\rho \gamma^\sigma \quad (90)$$

and just keeping the four γ matrices inside the traces. The diagrams where the pseudoscalar couples to squarks do not have such a vertex. They are however finite, such that a naively anticommuting γ_5 can be used at NLO. The chiral couplings at the quark-squark-gluino vertices are treated fully anticommuting to arrive at traces with one or no γ_5 matrix. Only the contributions with no additional γ_5 matrix contribute after applying the projector of Eq. (49). The projector yields a product of two Levi–Civita tensors that is defined as

$$\epsilon^{\mu\nu\rho\sigma} \epsilon_{\mu'\nu'\rho'\sigma'} = -\text{Det} \begin{bmatrix} g_{\mu'}^\mu & g_{\nu'}^\mu & g_{\rho'}^\mu & g_{\sigma'}^\mu \\ g_{\mu'}^\nu & g_{\nu'}^\nu & g_{\rho'}^\nu & g_{\sigma'}^\nu \\ g_{\mu'}^\rho & g_{\nu'}^\rho & g_{\rho'}^\rho & g_{\sigma'}^\rho \\ g_{\mu'}^\sigma & g_{\nu'}^\sigma & g_{\rho'}^\sigma & g_{\sigma'}^\sigma \end{bmatrix}, \quad (91)$$

where the metric tensors inside this determinant are treated as n -dimensional objects. This prescription avoids a splitting of γ matrices and loop momenta into 4- and $(n-4)$ -dimensional components. Since γ_5 as defined in Eq. (90) does not anticommute, an anomalous counterterm has to be added. However the genuine SUSY–QCD contributions to this counterterm vanish. In the 't Hooft–Veltman scheme, the metric tensors in this determinant are defined as strictly 4-dimensional objects so that the numerators of the loop integrals split into 4- and $(n-4)$ -dimensional pieces that have to be treated separately. To avoid additional anomalous counterterms we used anticommuting γ_5 matrices at the $Q\tilde{Q}\tilde{g}$ -vertices in this scheme as well. We found full agreement for both schemes. In addition, we have lifted the anti-commuting properties of the γ_5 matrices entering at the $Q\tilde{Q}\tilde{g}$ -vertices and found mismatches that require anomalous subtractions to restore the chiral properties. Finally, we have implemented the γ_5 scheme of Ref. [28] that gives up the cyclicity of the traces but keeps the full anti-commuting property of the γ_5 matrix. The cyclicity of the trace is equivalent to the arbitrary decision where we start to read the fermion lines. To resolve this, the scheme defines unambiguous reading points in each diagram relative to the external axial couplings. However, since we have no axial vector couplings in our diagrams, the only prescription we have to follow is that the reading point must be outside of subdivergences, e.g. in the fifth diagram of Fig. 5 the reading point must not be at the $g\tilde{g}\tilde{g}$ vertex. We found full agreement with the calculation in the Larin scheme as well.

Finally, we have reproduced the limit of large top, stop and gluino masses of Ref. [32] and found full agreement. Ref. [32] worked with Pauli–Villars regularization so that their Clifford algebra is defined in four dimensions strictly resulting in a fully anti-commuting γ_5 . That we have found full agreement with this calculation in the large-mass limit underlines the consistency of our results.

5.6 Adler–Bardeen Theorem

According to the analytical results of Ref. [32] the SUSY–QCD coefficient in the large SUSY-mass limit (keeping the quark mass small) is given by

$$\hat{\mathcal{C}}_{Q,SQCD}^A = -\frac{C_F}{2} \frac{M_{\tilde{g}}}{m_Q} \left(\frac{s_{2\theta_Q}}{2} - \frac{m_Q Y_Q}{m_{\tilde{Q}_1}^2 - m_{\tilde{Q}_2}^2} \right) \left(\frac{\rho_1}{1-\rho_1} \log \rho_1 - \frac{\rho_2}{1-\rho_2} \log \rho_2 \right) + \mathcal{O}(M_{SUSY}^{-2}), \quad (92)$$

with ρ_i as defined after Eq. (60). In this expression, we have focused just on the leading terms of the large-mass expansion, since this is the relevant contribution of the matching to a low-energy 2HDM. Moreover, in the expression above the Δ_Q terms are not subtracted, i.e. this is the result in terms of the LO Higgs coupling g_Q^A without Δ_Q -dressing. The coupling Y_Q is related to the squark coupling,

$$Y_Q = 2 \frac{g_{\tilde{Q}_1 \tilde{Q}_2}}{m_Q g_Q^A} = A_Q + \frac{\mu}{r_Q}. \quad (93)$$

Inserting the explicit expressions for $s_{2\theta_Q}$ and Y_Q one arrives at

$$\hat{\mathcal{C}}_{Q,SQCD}^A = -\Delta_Q \left(1 + \frac{1}{r_Q^2} \right) + \mathcal{O}(M_{SUSY}^{-2}). \quad (94)$$

Since the $At\bar{t}$ operator mixes with the $A\tilde{t}\tilde{t}^*$ operator the non-decoupling Δ_t contributions to the effective top Yukawa coupling are induced. Working with properly matched low-energy parameters, i.e. effective Yukawa couplings with Δ_Q contributions as in Eq. (82), this term is absorbed in the Yukawa couplings exactly so that the radiative corrections in the low-energy 2HDM with properly defined low-energy parameters are vanishing for the leading $\mathcal{O}(M_{SUSY}^0)$ term

$$\mathcal{C}_{Q,SQCD}^A = \mathcal{O}(M_{SUSY}^{-2}). \quad (95)$$

This is because in contrast to the MSSM, the chiral symmetry $\psi_Q \rightarrow e^{i\alpha\gamma_5}\psi_Q$ is only broken by the quark mass term in the effective 2HDM so that only the higher-order corrections to the proper matching of the low-energy 2HDM to the full MSSM contribute. Thus, in the low-energy limit the Adler–Bardeen theorem [17] is fulfilled⁵. Since radiative corrections still arise due to the higher-order corrections to the matching, the Adler–Bardeen theorem [17] builds a deep connection between the explicit structure of the radiative corrections in the full MSSM in the low-energy limit and the radiative corrections in the low-energy EFT. This result is in line with the result of Ref. [46] that the QCD corrections to the effective ggA Lagrangian in the HTL are vanishing if the strong coupling is chosen as the 5-flavour one, i.e. properly decoupling the top-quark contribution from the running of α_s or in other words using the properly matched low-energy α_s within pure 5-flavour QCD. This also implies that

⁵The Adler–Bardeen theorem is *not* valid for subleading $\mathcal{O}(M_{SUSY}^{-2})$ orders in the large SUSY-mass expansion with effective low-energy parameters as it also not valid for subleading $\mathcal{O}(m_t^{-2})$ orders of the large-top mass expansion of the pure QCD corrections.

in the large SUSY-mass limit (keeping the top mass small in comparison) no effective ggA operator is generated in the low-energy 2HDM at the dimension-5 level by integrating out the SUSY particles. The same is true as well for the bottom/sbottom contributions so that the SUSY particles do not generate a sbottom-induced effective ggA operator at leading $\mathcal{O}(M_{SUSY}^0)$ at all.

Another situation arises when the top quark is integrated out, i.e. assumed to be much heavier than the pseudoscalar A as well and *not* assumed to be much lighter than the other SUSY particles. In this case a dimension-5 operator contribution is generated on top of the HTL at LO due to the non-decoupling nature of the top quark as has already been observed for the leading $\mathcal{O}(G_F m_t^2)$ corrections to the effective Agg coupling [47]. Since the stops couple to the pseudoscalar in terms of the top Yukawa coupling as well, a new genuine dimension-5 contribution to the Agg coupling, on top of the contribution from the effective Yukawa coupling, emerges starting at NLO. This contribution can be related to the violation of the global Peccei–Quinn symmetry of the MSSM Lagrangian by the μ term [31, 32]. This leads to an extension of the related operator identity of the divergence of the axial-vector current by an additional operator involving the stop fields thus destroying the one-to-one correspondence between the pseudoscalar top-Yukawa coupling and the ABJ-anomaly operator and in this way the translation of the Adler–Bardeen theorem to the Agg operator. It follows that both the Δ_t terms and the genuine radiative corrections to the Agg coupling scale with the μ parameter [48]. Within the EFT view this has to be considered as higher-order corrections to the effective Agg operator in the combined HTL and large-SUSY-mass limit, i.e. higher-order corrections to the corresponding matching conditions that scale with μ .

6 Results

We are now in the position to present and discuss the final results of the NLO SUSY–QCD corrections to pseudoscalar $gg \rightarrow A$ production, but also to the pseudoscalar decays $A \rightarrow gg$ and $A \rightarrow \gamma\gamma$. For the numerical analysis we have adopted the M_h^{125} benchmark scenario [19] that is defined by the following on-shell parameters,

$$M_h^{125}: \quad M_{\tilde{Q}} = 1.5 \text{ TeV}, \quad M_{\tilde{\ell}_3} = 2 \text{ TeV}, \quad M_{\tilde{g}} = 2.5 \text{ TeV}, \\ M_1 = M_2 = 1 \text{ TeV}, \quad A_b = A_\tau = A_t = 2.8 \text{ TeV} + \mu/\text{tg}\beta, \quad \mu = 1 \text{ TeV}, \quad (96)$$

that have been used in the framework of the program HDECAY [49] with an iteration to determine the corresponding $\overline{\text{MS}}$ parameters accordingly. This proceeds along the lines discussed in Section 4. Here, $M_{\tilde{Q}}$ denotes the third-generation soft SUSY-breaking squark-mass parameters, $M_{\tilde{\ell}_3}$ the corresponding one for the sleptons and M_1, M_2 the soft SUSY-breaking gaugino-mass parameters for the bino and wino, respectively. For two representative

values of $\text{tg}\beta$, the related stop and sbottom masses amount to

$$\begin{aligned} \underline{\text{tg}\beta = 10} \\ m_{\tilde{t}_1} = 1340 \text{ GeV}, \quad m_{\tilde{t}_2} = 1662 \text{ GeV}, \quad m_{\tilde{b}_1} = 1496 \text{ GeV}, \quad m_{\tilde{b}_2} = 1508 \text{ GeV} \\ \underline{\text{tg}\beta = 40} \\ m_{\tilde{t}_1} = 1340 \text{ GeV}, \quad m_{\tilde{t}_2} = 1662 \text{ GeV}, \quad m_{\tilde{b}_1} = 1479 \text{ GeV}, \quad m_{\tilde{b}_2} = 1525 \text{ GeV}. \end{aligned} \quad (97)$$

Our numerical integration has been performed with the **VEGAS** subroutine [50] after preparing the integrands according to the methods described in Section 5. We have used up to $\mathcal{O}(10^9)$ points for the 5-dimensional **VEGAS** integration, with imaginary parts $\bar{\epsilon}$ of Eq. (53) up to the order of 10^{-3} above the virtual thresholds $(Q\bar{Q}, \tilde{Q}_1\bar{\tilde{Q}}_2, \tilde{Q}_2\bar{\tilde{Q}}_1)$ for $Q = t, b$. The numerical integration errors of our final results rank below the 10^{-2} -level for the final coefficients $\mathcal{C}_{Q,SQCD}^A$ of Eq. (51) and $\mathcal{D}_{Q,SQCD}^A$ of Eq. (14) for both the top- and bottom-induced corrections. This has been achieved with less than a week of CPU time for each individual M_A point.

6.1 Gluon Fusion $gg \rightarrow A$

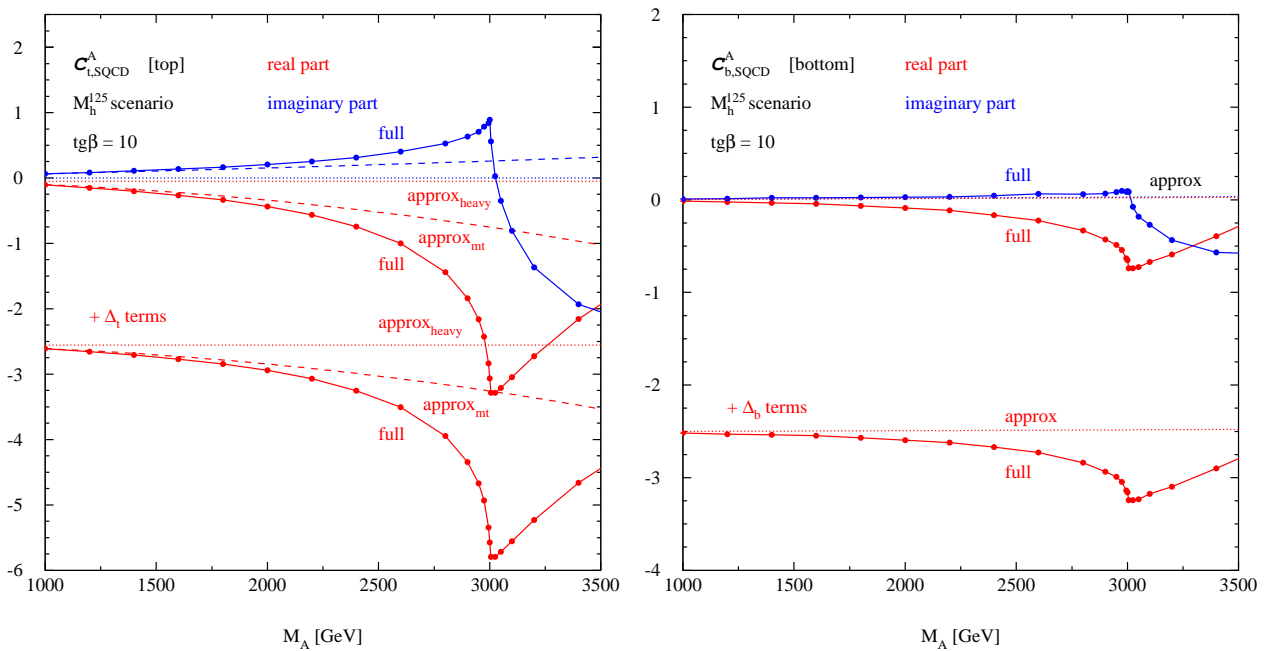


Figure 6: *The genuine SUSY-QCD corrections to $gg \rightarrow A$ normalized to the LO top and bottom quark form factors for $\text{tg}\beta = 10$ in the M_h^{125} benchmark scenario. Real part: red, imaginary part: blue, compared to the approximate calculations of Ref. [32] (dashed lines). The dotted lines for the stop contributions correspond to the combined limit of large top and SUSY masses.*

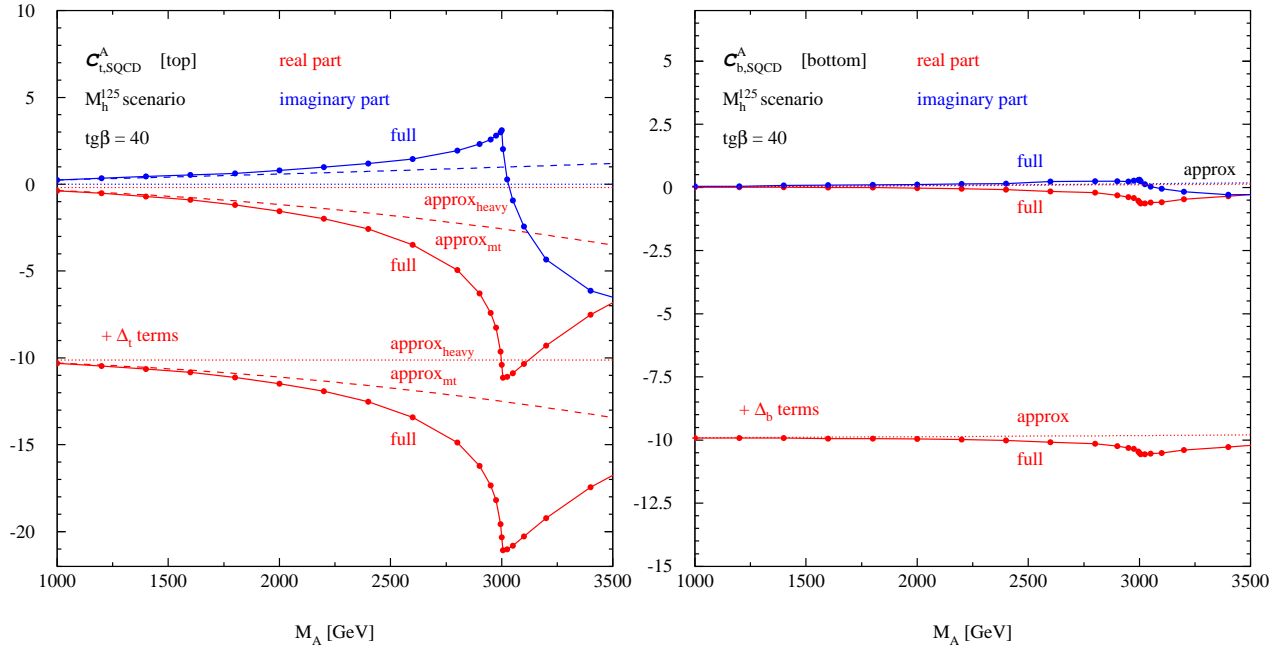


Figure 7: *The same as Fig. 6, but for $\tan\beta = 40$.*

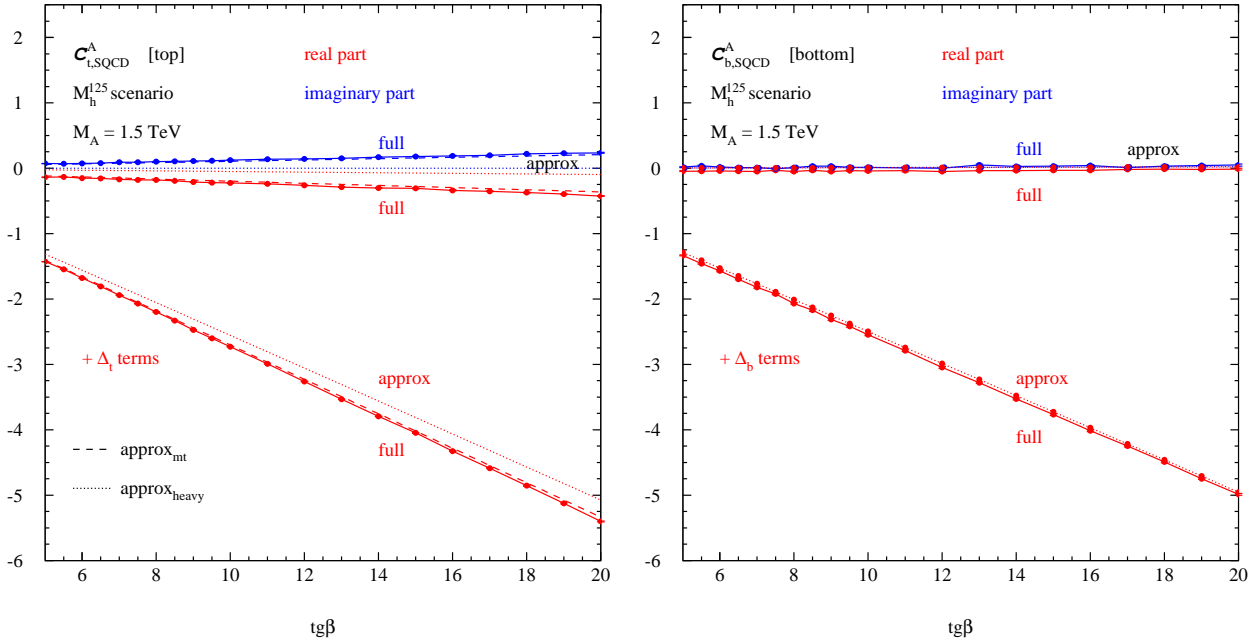


Figure 8: *The same as Fig. 6, but as a function of $\tan\beta$ for $M_A = 1.5$ TeV.*

As a starting point, the perturbative NLO coefficients $\mathcal{C}_{Q,SQCD}^A$ are displayed in Figs. 6 and 7 as a function of the pseudoscalar mass M_A for $\text{tg}\beta$ values of 10 and 40, respectively. In these figures, we show the approximate calculations of Ref. [32] as well, i.e. for the stop contribution both approximations of the combined heavy-top/SUSY limit ('approx_{heavy}') and the pure large SUSY-mass limit ('approx_{mt}'), while for the sbottom contribution only the large SUSY-mass limit ('approx') is phenomenologically relevant and shown. The full calculation agrees well with the former approximate calculations for smaller pseudoscalar masses in both the stop and sbottom cases. However, we observe sizeable and increasingly relevant deviations for pseudoscalar masses approaching or exceeding the virtual squark threshold⁶. Moreover, we display the results of the NLO coefficients for the two cases of absorbing the $\Delta_{t/b}$ terms in the corresponding Yukawa couplings and the opposite. It is clearly visible that the $\Delta_{t/b}$ terms approximate the full results quite well for smaller pseudoscalar masses M_A so that the results after subtracting them turn out to be quite small. These subtracted results represent the SUSY-remainder, i.e. the contributions beyond the leading parts corresponding to the effective top and bottom Yukawa couplings. It is obvious that the absorption of these contributions leads to a much better perturbative behaviour thus corroborating the effective Yukawa-coupling approach. This is further underlined by the $\text{tg}\beta$ dependence of the stop and sbottom contributions shown in Fig. 8 for a pseudoscalar mass $M_A = 1.5$ TeV. The description of the SUSY-QCD corrected cross section in terms of the effective low-energy top- and bottom-Yukawa couplings leads to a moderate SUSY-remainder at NLO as long as the pseudoscalar Higgs mass does not approach the virtual stop/sbottom thresholds. At and beyond these virtual thresholds, the SUSY-remainders turn out to be sizeable.

As the next step, we analyze the SUSY-QCD corrections to the hadronic cross section of pseudoscalar Higgs-boson production via gluon fusion. The effect of the corrections on the K -factor at the hadronic level, which is defined as the ratio between the NLO and LO cross sections, is discussed first. We adopt the MSHT20nlo_as118 parton density functions and perform the analysis for a c.m. energy of 13 TeV at the LHC. Fig. 9 exhibits the K -factor for $\text{tg}\beta = 10, 40$ with effective top- and bottom-Yukawa couplings for the QCD part of the cross section and for the corresponding results of the previous approximate calculations. The QCD part of the K -factors shows the usual sizeable NLO corrections of about 30–50%, while the additional SUSY-QCD remainder turns out to be small or moderate. The comparison implies that effects beyond the approximation become relevant when approaching the virtual stop/sbottom thresholds and above as expected.

These K -factors can be translated to the hadronic production cross sections of pseudoscalar Higgs bosons via gluon fusion as shown in Fig. 10 for two values of $\text{tg}\beta = 10, 40$. For the effective bottom-Yukawa couplings, we include the full set of NNLO corrections [51] to lift the accuracy of the factorizing and dominant contributions to the NNLO level, while for the effective top-Yukawa coupling we use the NLO expression in the effective field-theory framework. Here, we present the QCD-corrected cross sections without the effective top- and bottom-Yukawa couplings, i.e. without any genuine SUSY-QCD corrections and the approximate and full SUSY-QCD corrected cross sections with the effective Yukawa couplings

⁶The kink structure at the heavy squark threshold is in line with the S -wave but \mathcal{CP} -odd behaviour of $\tilde{q}_1\bar{\tilde{q}}_2$ and $\tilde{q}_2\bar{\tilde{q}}_1$ pairs of different squarks close to the threshold.

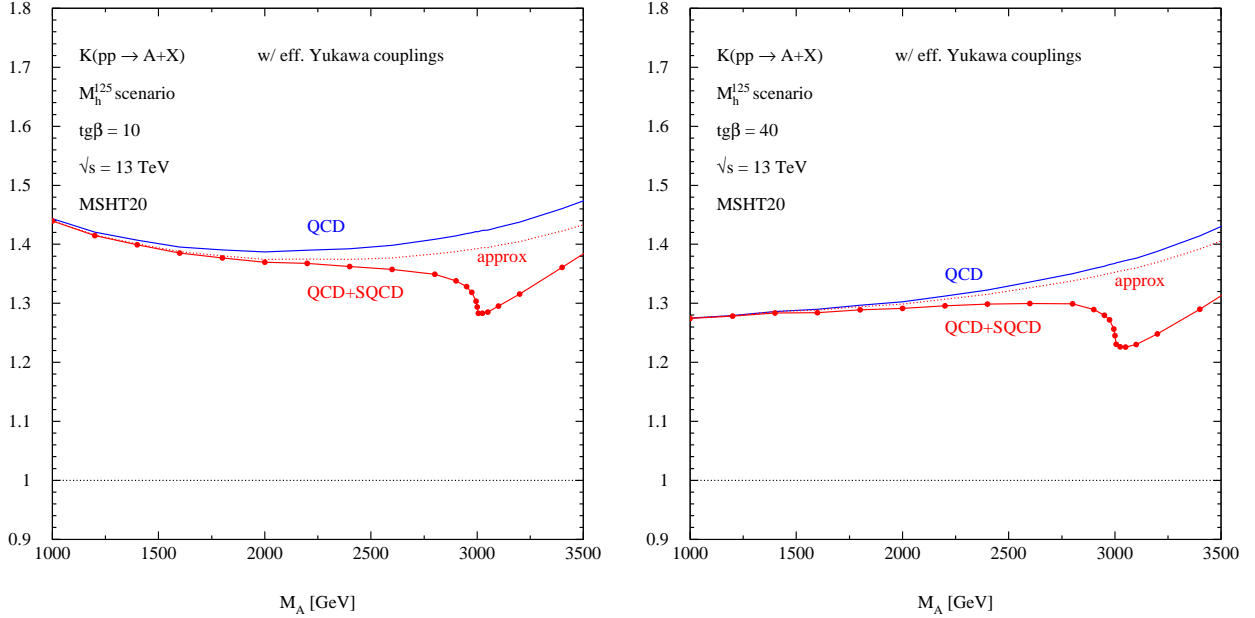


Figure 9: *The K -factors of the QCD and genuine SUSY-QCD corrections for the LHC with $\text{tg}\beta = 10, 40$ and a c.m. energy of 13 TeV. As parton density functions the MSHT20 sets have been used. The renormalization and factorization scales have been chosen as $\mu_R = \mu_F = M_A/2$.*

as discussed in the previous section. The comparison of the full QCD-corrected cross section (blue line) and the full QCD + SUSY-QCD corrected cross section (red line) supports the high relevance of the SUSY-QCD corrections in total, while the SUSY-remainder plays a role close or above the virtual stop- and sbottom thresholds.

6.2 The Gluonic Decay $A \rightarrow gg$

The same virtual coefficient as for $gg \rightarrow A$ contributes to the genuine SUSY-QCD corrections of the gluonic pseudoscalar Higgs decay $A \rightarrow gg$ according to Eq. (11). The relative QCD and SUSY-QCD corrections to the gluonic decay width are shown in Fig. 11 with the use of effective top and bottom Yukawa couplings. It is clearly visible that the bulk of the genuine SUSY-QCD corrections can be absorbed by the effective top and bottom Yukawa couplings including $\Delta_{t,b}$ contributions. The SUSY-remainder is relevant in regions where finite squark-mass effects become relevant, i.e. close or above the related virtual thresholds.

The corresponding partial decay widths $\Gamma(A \rightarrow gg)$ are shown in Fig. 12 for $\text{tg}\beta = 10, 40$, using effective top and bottom Yukawa couplings for the SUSY-QCD-corrected decay widths, but LO couplings without $\Delta_{t,b}$ terms for the LO and QCD-corrected decay widths. The SUSY-QCD corrections are treated in the same way as for the production cross sections, i.e. Δ_b terms at two-loop order and Δ_t contributions at one-loop level. The main effect of the genuine SUSY-QCD corrections emerges from the factorizing $\Delta_{b,t}$ corrections to the

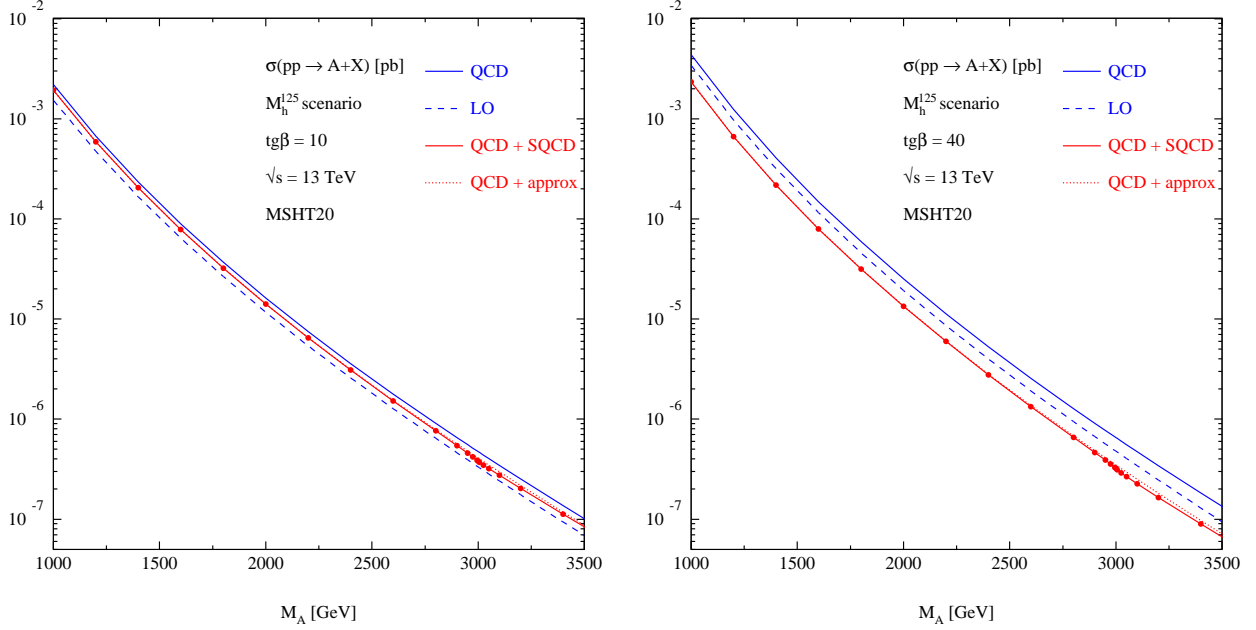


Figure 10: *The pseudoscalar production cross section via gluon-fusion at the LHC with $\text{tg}\beta = 10$ (left) and $\text{tg}\beta = 40$ (right) and a c.m. energy of 13 TeV at LO, NLO QCD and including the genuine SUSY–QCD corrections involving effective Yukawa couplings. The LO and NLO QCD corrected cross sections are shown without effective Yukawa couplings. As parton density functions the MSHT20 sets have been used. The renormalization and factorization scales have been chosen as $\mu_R = \mu_F = M_A/2$.*

Yukawa couplings. The comparison of the pure NLO QCD prediction (blue curve) and the SUSY–QCD corrected one (red curve) indicates the large size of SUSY–QCD corrections at NLO for the partial width.

6.3 The Photonic Decay $A \rightarrow \gamma\gamma$

The virtual SUSY–QCD corrections to the photonic decay width of $A \rightarrow \gamma\gamma$ emerge from the first four diagrams of Fig. 5 after adjusting the related coupling and color factors and replacing the two external gluons by photons. The normalized coefficient of the SUSY–QCD corrections with and without absorption of the $\Delta_{t,b}$ terms is shown in Figs. 13 and 14 for two values of $\text{tg}\beta = 10, 40$. As in the gluonic case the Δ_t and Δ_b contributions determine the dominant part of the SUSY–QCD corrections that can be absorbed in the effective top and bottom Yukawa couplings of Eq. (82). The SUSY–QCD remainder turns out to be small apart from the regions closer to the virtual stop and sbottom thresholds. The partial decay widths of $A \rightarrow \gamma\gamma$ are shown in Fig. 15 for the different levels of perturbative orders. The LO and NLO QCD corrected widths are shown in blue, while the approximate and full SUSY–QCD-corrected ones are displayed in red. As in the previous cases it is clearly visible that the bulk of the genuine SUSY–QCD corrections can be absorbed by the corresponding

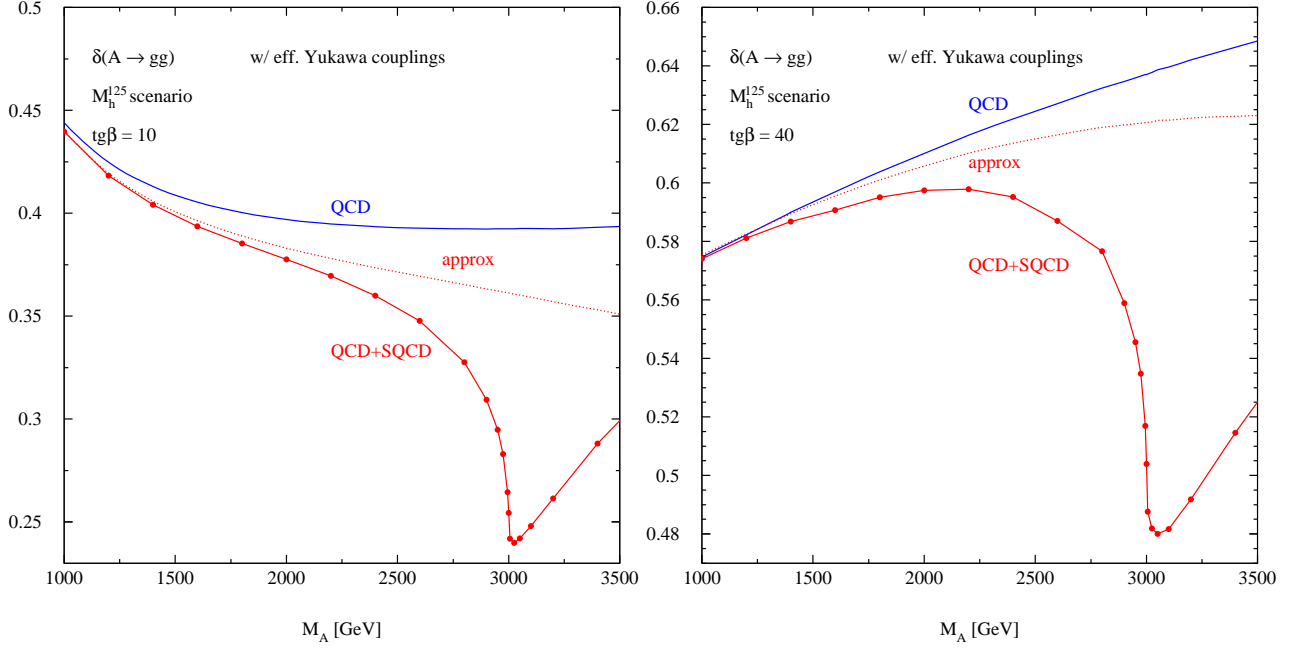


Figure 11: *Relative radiative corrections, defined as $\Gamma = \Gamma_{LO}(1 + \delta)$, to the gluonic pseudoscalar decay width as a function of the pseudoscalar mass M_A for $\text{tg}\beta = 10$ (left) and $\text{tg}\beta = 40$ (right) at NLO QCD and including the genuine SUSY-QCD corrections involving effective Yukawa couplings. The renormalization scale has been chosen as $\mu_R = M_A$.*

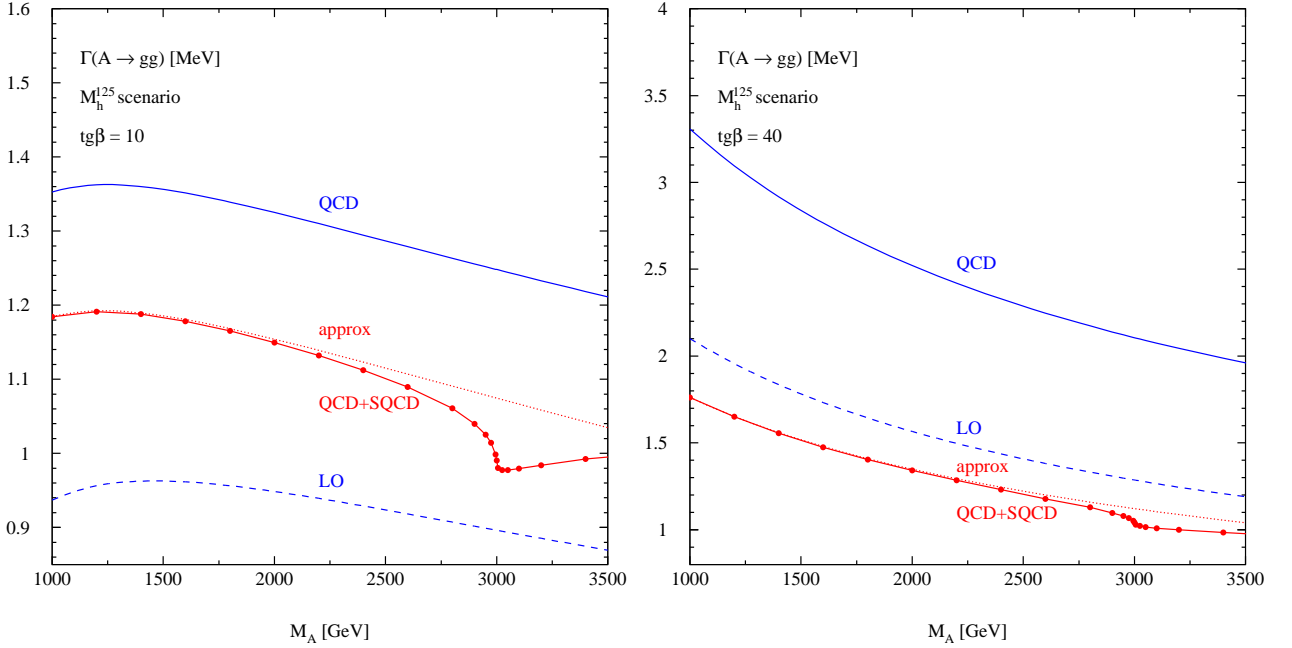


Figure 12: *Partial decay widths $\Gamma(A \rightarrow gg)$ as a function of the pseudoscalar mass M_A for $\text{tg}\beta = 10$ (left) and $\text{tg}\beta = 40$ (right) at NLO QCD and including the genuine SUSY-QCD corrections involving effective Yukawa couplings. The renormalization scale has been chosen as $\mu_R = M_A$.*

effective top and bottom Yukawa couplings leaving a sizeable SUSY-remainder in regions only where squark-mass effects become relevant. The extended peaking structure around a pseudoscalar mass of 2 TeV originates from the two chargino thresholds that are not affected by corrections due to strong interactions. It should be noted that the same corrections are valid for the reverse process $\gamma\gamma \rightarrow A$ as well, which could be probed at a potential future high-energy $\gamma\gamma$ -collider.

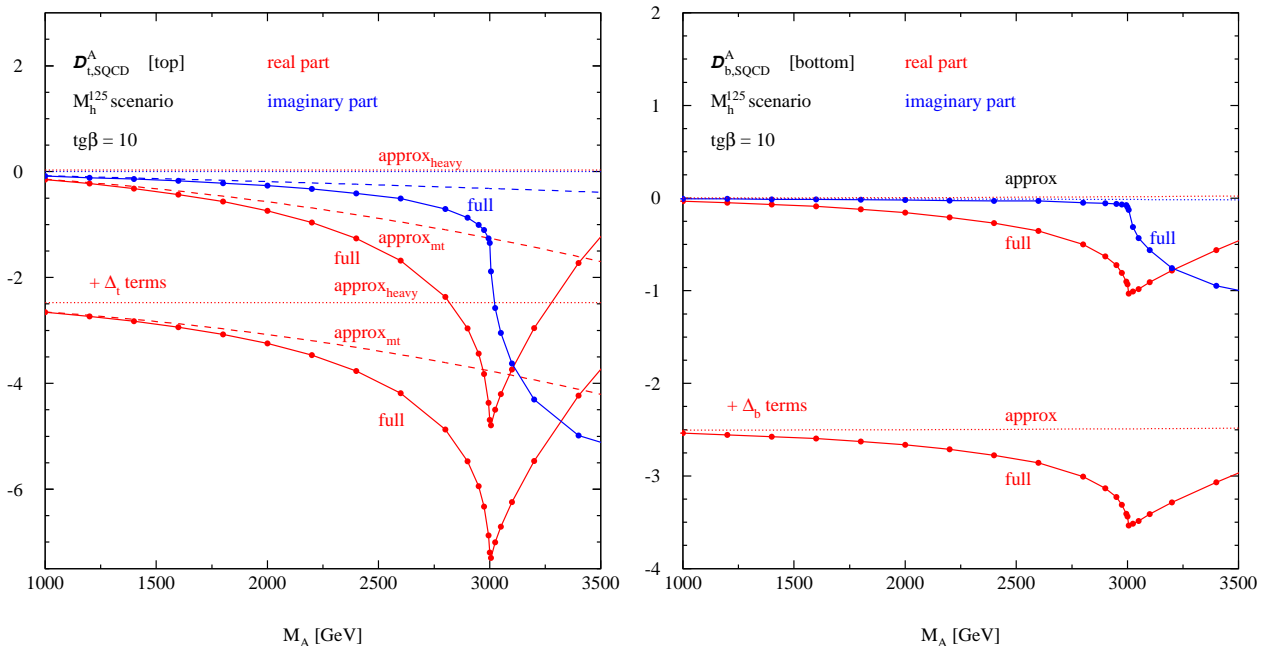


Figure 13: *The genuine SUSY-QCD corrections to $A \rightarrow \gamma\gamma$ normalized to the LO top and bottom quark form factors for $\text{tg}\beta = 10$ in the M_h^{125} benchmark scenario. Real part: red, imaginary part: blue, compared to the Abelian part of the approximate calculations of Ref. [32] (dashed lines). The dotted lines for the stop contributions correspond the combined limit of large top and SUSY masses.*

7 Conclusions

We have calculated the full SUSY-QCD corrections to pseudoscalar Higgs-boson production via gluon fusion $gg \rightarrow A$ within the MSSM at hadron colliders. We implemented the virtual stop and sbottom sector at the NLO level to be in line with the necessities for the corresponding scalar Higgs-boson production cross sections via gluon fusion $gg \rightarrow h, H$. We have analyzed pseudoscalar Higgs-boson production with respect to the introduction of effective low-energy top and bottom Yukawa couplings, i.e. the couplings within the low-energy 2HDM after integrating out the strongly interacting SUSY particles (stops, sbottoms and gluinos). We found that the bulk of the NLO corrections can be absorbed in these effective Yukawa couplings, while the SUSY-remainder is of moderate size, being significant

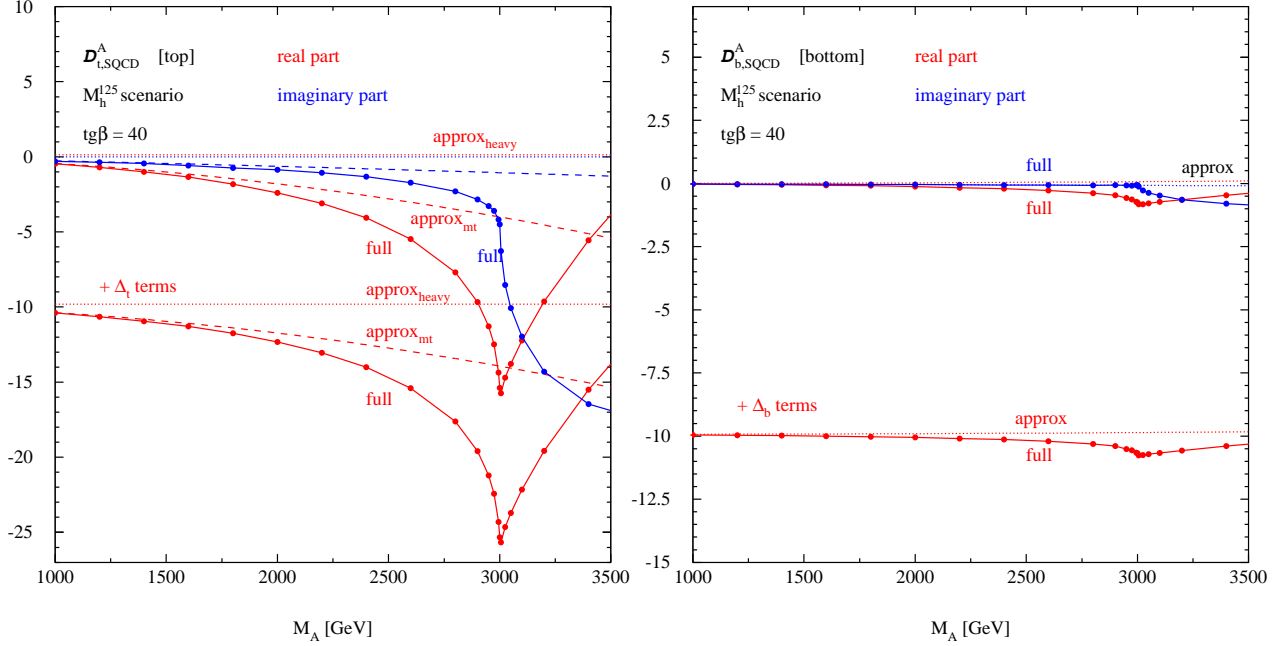


Figure 14: *The same as Fig. 13, but for $\text{tg}\beta = 40$.*

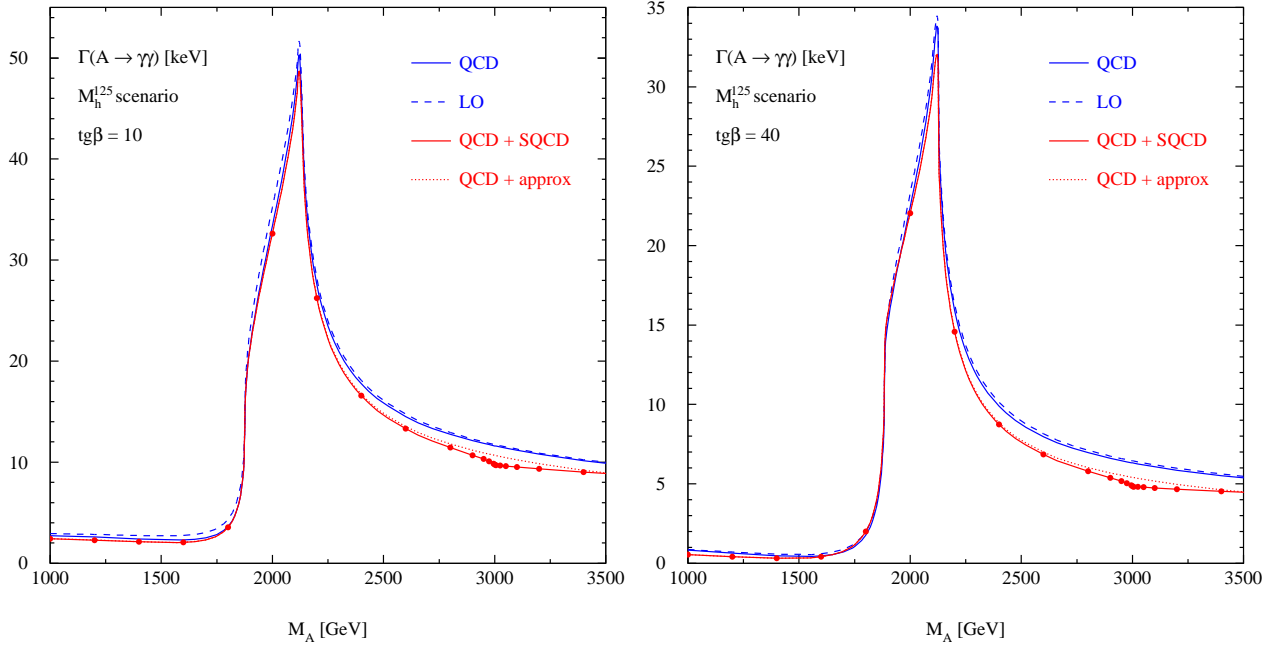


Figure 15: *The partial decay width of $A \rightarrow \gamma\gamma$ for two values of $\text{tg}\beta = 10, 40$ in the M_h^{125} benchmark scenario at LO and NLO QCD (blue) and including the genuine SUSY-QCD corrections involving effective Yukawa couplings (red).*

close or above virtual squark thresholds. We have analyzed the corrections in the context of the Adler-Bardeen theorem and found that this theorem is fulfilled in the large SUSY-mass limit, if the observable is expressed in terms of properly matched low-energy parameters, i.e. top- and bottom-Yukawa couplings. The analogous results have also been obtained for the related rare pseudoscalar Higgs-boson decays $A \rightarrow gg, \gamma\gamma$ that, however, only play a minor role in phenomenological analyses at hadron colliders. This work completes the full NLO QCD calculation for pseudoscalar MSSM Higgs production and decay into gluonic and photonic final states and thus serves as a basis for the corresponding theoretical predictions.

Acknowledgements.

We are grateful to J. Reuter for private communication on the Adler–Bardeen theorem. The research of T.T.D.N. and M.M. was supported by the Deutsche Forschungsgemeinschaft (DFG, German Research Foundation) under grant 396021762 - TRR 257. The work of L.F. has been supported by the Swiss National Science Foundation (SNSF).

References

- [1] G. Aad *et al.* [ATLAS Collaboration], Phys. Lett. **B716** (2012) 1; S. Chatrchyan *et al.* [CMS Collaboration], Phys. Lett. **B716** (2012) 30.
- [2] P. Higgs, Phys. Lett. **12** (1964) 132, Phys. Rev. Lett. **13** (1964) 508 and Phys. Rev. **145** (1966) 1156; F. Englert and R. Brout, Phys. Rev. Lett. **13** (1964) 321; G. Guralnik, C. Hagen and T. Kibble, Phys. Rev. Lett. **13** (1964) 585; T.W.B. Kibble, Phys. Rev. **155** (1967) 1554; S. Weinberg, Phys. Rev. Lett. **19** (1967) 1264.
- [3] G. 't Hooft, Nucl. Phys. **B35** (1971) 167; G. 't Hooft and M.J.G. Veltman, Nucl. Phys. **B44** (1972) 189.
- [4] G. Aad *et al.* [ATLAS and CMS Collaborations], JHEP **1608** (2016) 045; G. Aad *et al.* [ATLAS Collaboration], ATLAS-CONF-2019-005; A.M. Sirunyan *et al.* [CMS Collaboration], JHEP **01** (2021) 148.
- [5] C.H. Llewellyn Smith, Phys. Lett. **46B** (1973) 233; J.M. Cornwall, D.N. Levin and G. Tiktopoulos, Phys. Rev. **D10** (1974) 1145 [Erratum-ibid. **D11** (1975) 972]; B.W. Lee *et al.*, Phys. Rev. Lett. **38** (1977) 883 and Phys. Rev. **D16** (1977) 1519.
- [6] E. Gildener and S. Weinberg, Phys. Rev. **D13** (1976) 3333; S. Weinberg, Phys. Rev. **D13** (1976) 974 and Phys. Rev. **D19** (1979) 1277; L. Susskind, Phys. Rev. **D20** (1979) 2619.
- [7] T.D. Lee, Phys. Rev. **8** (1973) 1226; J.F. Gunion and H.E. Haber, Phys. Rev. **D67** (2003) 075019; G.C. Branco, P.M. Ferreira, L. Lavoura, M.N. Rebelo, M. Sher and J.P. Silva, Phys. Rept. **516** (2012) 1.
- [8] P. Fayet, Nucl. Phys. B **90** (1975) 104, Phys. Lett. B **64** (1976) 159 and Phys. Lett. B **69** (1977) 489; P. Fayet and S. Ferrara, Phys. Rept. **32** (1977) 249; H. P. Nilles, Phys. Rept. **110** (1984) 1; R. Barbieri, Riv. Nuovo Cim. **11N4** (1988) 1.

- [9] H. E. Haber and G. L. Kane, Phys. Rept. **117** (1985) 75.
- [10] E. Witten, Phys. Lett. **105B** (1981) 267.
- [11] S. Dimopoulos, S. Raby and F. Wilczek, Phys. Rev. **D24** (1981) 1681; L.E. Ibanez and G.G. Ross, Phys. Lett. **105B** (1981) 439.
- [12] H. Goldberg, Phys. Rev. Lett. **50** (1983) 1419 [Erratum-ibid. **103** (2009) 099905]; J.R. Ellis et al., Nucl. Phys. **B238** (1984) 453.
- [13] L.E. Ibanez and G.G. Ross, Phys. Lett. **110B** (1982) 215.
- [14] P. Fayet, Nucl. Phys. **B90** (1975) 104, Phys. Lett. **B64** (1976) 159 and Phys. Lett. **B69** (1977) 489; N. Sakai, Z. Phys. **C11** (1981) 153; K. Inoue et al., Prog. Theor. Phys. **67** (1982) 1889, Prog. Theor. Phys. **68** (1982) 927 [Erratum-ibid. **70** (1983) 330] and Prog. Theor. Phys. **71** (1984) 413.
- [15] S. L. Adler, Phys. Rev. **177** (1969) 2426; J. S. Bell and R. Jackiw, Nuovo Cim. **A60** (1969) 47.
- [16] See e.g. P. Slavich, S. Heinemeyer, E. Bagnaschi, H. Bahl, M. Goodsell, H. E. Haber, T. Hahn, R. Harlander, W. Hollik and G. Lee, *et al.* Eur. Phys. J. **C81** (2021) no.5, 450.
- [17] S. L. Adler and W. A. Bardeen, Phys. Rev. **182** (1969) 1517.
- [18] Z. Kunszt and F. Zwirner, Nucl. Phys. **B385** (1992) 3; V. D. Barger, M. S. Berger, A. L. Stange and R. J. N. Phillips, Phys. Rev. **D45** (1992) 4128.
- [19] E. Bagnaschi *et al.*, Eur. Phys. J. **C79** (2019) no.7, 617.
- [20] H. M. Georgi, S. L. Glashow, M. E. Machacek and D. V. Nanopoulos, Phys. Rev. Lett. **40** (1978) 692.
- [21] R. Raitio and W.W. Wada, Phys. Rev. **D19** (1979) 941; J. N. Ng and P. Zakarauskas, Phys. Rev. **D29** (1984) 876; Z. Kunszt, Nucl. Phys. **B247** (1984) 339; J. F. Gunion, Phys. Lett. **B261** (1991) 510; W. J. Marciano and F. E. Paige, Phys. Rev. Lett. **66** (1991) 2433; D. A. Dicus and S. Willenbrock, Phys. Rev. **D39** (1989) 751.
- [22] J. F. Gunion, H. E. Haber, G. L. Kane and S. Dawson, Front. Phys. **80** (2000) 1.
- [23] M. Spira, A. Djouadi, D. Graudenz and P. M. Zerwas, Nucl. Phys. **B453** (1995) 17.
- [24] M. Spira, A. Djouadi, D. Graudenz and P. M. Zerwas, Phys. Lett. **B318** (1993) 347.
- [25] R. Harlander and P. Kant, JHEP **0512** (2005) 015; C. Anastasiou, S. Beerli, S. Bucherer, A. Daleo and Z. Kunszt, JHEP **0701** (2007) 082; U. Aglietti, R. Bonciani, G. Degrossi and A. Vicini, JHEP **0701** (2007) 021.

- [26] G. 't Hooft and M. J. G. Veltman, Nucl. Phys. **B44** (1972) 189; P. Breitenlohner and D. Maison, Commun. Math. Phys. **52** (1977) 11.
- [27] S. A. Larin, Phys. Lett. **B303** (1993) 113.
- [28] J. G. Körner, D. Kreimer and K. Schilcher, Z. Phys. **C54** (1992) 503; D. Kreimer, hep-ph/9401354.
- [29] R.V. Harlander and W. B. Kilgore, JHEP **10** (2002), 017; C. Anastasiou and K. Melnikov, Phys. Rev. **D67** (2003) 037501; V. Ravindran, J. Smith and W. L. van Neerven, Nucl. Phys. **B665** (2003), 325-366.
- [30] M. Krämer, E. Laenen and M. Spira, Nucl. Phys. **B511** (1998) 523.
- [31] R. V. Harlander and F. Hofmann, JHEP **0603** (2006) 050; R. V. Harlander, F. Hofmann and H. Mantler, JHEP **1102** (2011) 055.
- [32] G. Degrassi, S. Di Vita and P. Slavich, JHEP **1108** (2011) 128.
- [33] T. Liu and A. A. Penin, Phys. Rev. Lett. **119** (2017) no.26, 262001 and JHEP **11** (2018), 158; C. Anastasiou and A. Penin, JHEP **07** (2020), 195 [erratum: JHEP **01** (2021), 164]; Z. L. Liu, B. Mecaj, M. Neubert and X. Wang, Phys. Rev. **D104** (2021) no.1, 014004.
- [34] K. G. Chetyrkin, B. A. Kniehl, M. Steinhauser and W.A. Bardeen, Nucl. Phys. **B535** (1998) 3.
- [35] S. G. Gorishnii, A. L. Kataev, S. A. Larin and L. R. Surguladze, Mod. Phys. Lett. **A5** (1990) 2703 and Phys. Rev. **D43** (1991) 1633; K. G. Chetyrkin, Phys. Lett. **B404** (1997) 161; J. A. M. Vermaseren, S. A. Larin and T. van Ritbergen, Phys. Lett. **B405** (1997) 327.
- [36] N. Gray, D. J. Broadhurst, W. Grafe and K. Schilcher, Z. Phys. **C48** (1990), 673.
- [37] E. Accomando, G. Chachamis, F. Fugel, M. Spira and M. Walser, Phys. Rev. **D85** (2012) 015004.
- [38] A. Brignole, G. Degrassi, P. Slavich and F. Zwirner, Nucl. Phys. **B643** (2002) 79; S. Heinemeyer, W. Hollik, H. Rzehak and G. Weiglein, Eur. Phys. J. **C39** (2005) 465; S. Heinemeyer, H. Rzehak and C. Schappacher, Phys. Rev. **D82** (2010), 075010; G. Degrassi and P. Slavich, JHEP **11** (2010) 044.
- [39] G. 't Hooft and M.J.G. Veltman, Nucl. Phys. **B153** (1979) 365; G. Passarino and M.J.G. Veltman, Nucl. Phys. **B160** (1979) 151.
- [40] S.P. Martin and M.T. Vaughn, Phys. Lett. **B318** (1993) 331.

- [41] A. Bartl, H. Eberl, K. Hidaka, T. Kon, W. Majerotto and Y. Yamada, Phys. Lett. **B402** (1997) 303; A. Arhrib, A. Djouadi, W. Hollik and C. Jünger, Phys. Rev. **D57** (1998) 5860; H. Eberl, K. Hidaka, S. Kraml, W. Majerotto and Y. Yamada, Phys. Rev. **D62** (2000) 055006.
- [42] R. V. Harlander, S. Liebler and H. Mantler, Comput. Phys. Commun. **184** (2013), 1605.
- [43] J. Baglio, F. Campanario, S. Glaus, M. Mühlleitner, M. Spira and J. Streicher, Eur. Phys. J. **C79** (2019) no.6, 459; J. Baglio, F. Campanario, S. Glaus, M. Mühlleitner, J. Ronca, M. Spira and J. Streicher, JHEP **04** (2020), 181; J. Baglio, F. Campanario, S. Glaus, M. Mühlleitner, J. Ronca and M. Spira, Phys. Rev. **D103** (2021) no.5, 056002.
- [44] A. Djouadi, M. Spira, J.J. van der Bij and P.M. Zerwas, Phys. Lett. **B257** (1991), 187-190; M. Spira, A. Djouadi and P. M. Zerwas, Phys. Lett. **B276** (1992), 350-353; M. Mühlleitner and M. Spira, Nucl. Phys. **B790** (2008), 1-27 M. Mühlleitner, H. Rzehak and M. Spira, PoS **RADCOR2009** (2010) 043 and DESY-PROC-2010-01.
- [45] J. Guasch, P. Häfliger and M. Spira, Phys. Rev. **D68** (2003) 115001.
- [46] K.G. Chetyrkin, B.A. Kniehl, M. Steinhauser and W.A. Bardeen, Nucl. Phys. **B535** (1998) 3.
- [47] J. Brod, F. Fugel and B. A. Kniehl, Phys. Rev. **D78** (2008) 011303 and Nucl. Phys. **B807** (2009) 188.
- [48] L. Fritz, PhD thesis, University of Zurich, 2022.
- [49] A. Djouadi, J. Kalinowski and M. Spira, Comput. Phys. Commun. **108** (1998) 56; A. Djouadi, M. M. Mühlleitner and M. Spira, Acta Phys. Polon. **B38** (2007) 635; A. Djouadi, J. Kalinowski, M. Mühlleitner and M. Spira, Comput. Phys. Commun. **238** (2019) 214.
- [50] G. P. Lepage, preprint CLNS-80/447.
- [51] D. Noth and M. Spira, Phys. Rev. Lett. **101**, 181801 (2008) and JHEP **1106**, 084 (2011); L. Mihaila and C. Reisser, JHEP **1008**, 021 (2010); A. Crivellin and C. Greub, Phys. Rev. **D87** (2013) 015013 Erratum: [Phys. Rev. **D87** (2013) 079901]; M. Ghezzi, S. Glaus, D. Müller, T. Schmidt and M. Spira, Eur. Phys. J. **C81** (2021) no.3, 259.